

3 μm water vapor self- and foreign-continuum: new method for determination and new insights into the self-continuum

Article

Accepted Version

Creative Commons: Attribution-Noncommercial-No Derivative Works 4.0

Birk, M., Wagner, G., Loos, J. and Shine, K. P. (2020) 3 μm water vapor self- and foreign-continuum: new method for determination and new insights into the self-continuum. *Journal of Quantitative Spectroscopy and Radiative Transfer*, 253. 107134. ISSN 0022-4073 doi: <https://doi.org/10.1016/j.jqsrt.2020.107134> Available at <http://centaur.reading.ac.uk/91123/>

It is advisable to refer to the publisher's version if you intend to cite from the work. See [Guidance on citing](#).

Published version at: <http://dx.doi.org/10.1016/j.jqsrt.2020.107134>

To link to this article DOI: <http://dx.doi.org/10.1016/j.jqsrt.2020.107134>

Publisher: Elsevier

All outputs in CentAUR are protected by Intellectual Property Rights law, including copyright law. Copyright and IPR is retained by the creators or other

copyright holders. Terms and conditions for use of this material are defined in the [End User Agreement](#).

www.reading.ac.uk/centaur

CentAUR

Central Archive at the University of Reading

Reading's research outputs online

1 **3 μm water vapor self- and foreign-continuum: New method**
2 **for determination and new insights into the self-continuum**

3 M. Birk^{a*}, G. Wagner^a, J. Loos^a, K.P. Shine^b

4

5 ^aRemote Sensing Technology Institute, German Aerospace Center (DLR), D-82234 Wessling, Germany

6 ^bDepartment of Meteorology, University of Reading, Earley Gate, Reading RG6 6BB, UK

7

8

9 *Corresponding author: Manfred Birk, manfred.birk@dlr.de, +498153283084

10

11

12 Email addresses of all authors

13 manfred.birk@dlr.de

14 georg.wagner@dlr.de

15 joep.loos@web.de

16 k.p.shine@reading.ac.uk, Orcid ID 0000-0003-2672-9978

17 **Abstract**

18 The H₂O self- and foreign- in-band continua in the region 3400-3900 cm⁻¹ were experimentally
19 determined for 296 and 353 K from multispectrum fitting results of line parameters using the Hartmann-
20 Tran line profile (HTP) and Rosenkranz line mixing. The continua were extracted from the baselines
21 which were determined in the microwindow-based multispectrum fits. Continua were then obtained by
22 simultaneous fitting of all baselines from measurements containing continuum information. The self-
23 continuum at 296 K was determined from self-broadened measurements and agrees with that
24 determined from air broadened measurements. The overall shape and strength of the new self-
25 continuum agrees with the CAVIAR results between 3600 and 3800 cm⁻¹ but differences exceed the
26 stated uncertainties at higher and lower wavenumbers. Moreover, the new self-continuum is much
27 smoother, has no gaps and is obtained with a high resolution of 2.4 cm⁻¹. The self-continuum was fitted
28 as sum of modeled bound and quasi-bound dimer spectra. From rotational constants, the bound dimer
29 parallel and perpendicular band shapes of the near prolate symmetric top molecule were calculated and
30 used as kernels to fit fundamental wavenumbers, relative band intensities and partitioning of parallel
31 and perpendicular band type, while the integral of the band intensities of the four fundamentals was
32 fixed to published experimental/theoretical data. A dimerization constant for the bound dimer of
33 $K_{Db}=0.026(2)$ atm⁻¹ and the quasi-bound dimer of $K_{Dq}=0.044(5)$ atm⁻¹ was derived from the fits.

34 The foreign-continuum has no gaps, a spectral resolution of 6-16 cm⁻¹, and is about 40% smaller than the
35 MT_CKD3.2 continuum model. It has a distinctly different shape showing a pronounced P-Q-R branch
36 structure. The foreign-continuum shape is narrower than the monomer band shape which is also true for
37 the MT_CKD3.2 continuum model. The CAVIAR foreign-continuum is much noisier but on average is in
38 good agreement with the new measurements.

39 **Keywords**

40 Water vapor, self-continuum, foreign-continuum, Fourier Transform spectroscopy, water dimer

41 **1. Introduction**

42 The water vapor continuum is absorption found in pure water vapor and water/air spectra which cannot
43 be attributed to Voigt based rotational or rovibrational water lines. There are two distinct contributions,
44 the self-continuum (SC) and the foreign-continuum (FC). While the SC optical depth is proportional to the
45 water pressure squared, the FC optical depth is proportional to the water pressure and the air (or other
46 broadening gas) pressure. The history of the continua is summarized for example in [Shine2012]. The
47 name continuum is related to the absence of high resolution features. It is rather weak when compared
48 to the typical rotational and rovibrational water vapor bands. In the following the MT_CKD continuum
49 will be introduced, the relevance of the continuum for climate and remote sensing discussed, and the
50 common method for extraction of the continuum briefly mentioned. While these subsections are more
51 general, the subsection about the experimental continuum data is focused on the near infrared region
52 close to the spectral range around 3 μm relevant to this work. In the final subsection the current
53 understanding of the physical background of the continuum is discussed.

54

55 **1.1 MT_CKD Continuum Model**

56 A commonly used parameterization of the continuum is the MT_CKD (Mlawer-Tobin_Clough-Kneizys-
57 Davies) continuum model [Mlawer2012]. The first versions of its predecessor, the CKD continuum model
58 [Clough1989], are based on older laboratory measurements mostly by Burch and co-workers
59 [Burch1982;Burch1984] in the 1980s in the range 330-2000 cm^{-1} (for details see [Clough1989]). The CKD
60 continuum model is constructed from uniformly modified Lorentzian profiles of the water lines listed in
61 the HITRAN database to fit the experimental continuum. Although the spectral range of the above
62 mentioned laboratory measurements is limited, the total range from 0 to 20000 cm^{-1} given by CKD model
63 is based on this line profile modification applied at all wavenumbers. For the FC and SC separately, there
64 is one line-profile function which is multiplied with the Voigt function of each line and contains a super-
65 Lorentzian and sub-Lorentzian region. The local lines in a $\pm 25 \text{ cm}^{-1}$ interval are omitted, except for a so-
66 called plinth/pedestal, which is the value of the Lorentz-line at $\pm 25 \text{ cm}^{-1}$ which is subtracted from the line

67 contribution within 25 cm^{-1} of line centre and added to the continuum. Contributions from all lines are
68 summed. Based on remote sensing results, the CKD continuum model was updated several times and
69 finally replaced by the MT_CKD formalism since the many changes could not be well represented by the
70 CKD formalism [Mlawer2012]. The MT_CKD continuum model is composed of two parts, an allowed term
71 and a so-called 'weak interaction' term. The allowed term covers the sub-Lorentzian part only while the
72 weak interaction term gives most of the in-band and, especially in case of the SC, also part of the in-
73 between band continuum. While the FC is treated as temperature independent, the rather strong
74 temperature dependence of the SC is extrapolated from experimental data in the range 296-338 K to
75 lower temperatures.

76
77 The tabulated MT_CKD SC model values are larger than the FC values. The maximum in-band SC values
78 for the ν_2 band around 1600 cm^{-1} and the ν_1/ν_3 bands around 3800 cm^{-1} are $5\text{-}6 \times 10^{-21} \text{ cm}^2 \text{ molecule}^{-1} \text{ atm}^{-1}$,
79 while the FC is about 11 times weaker. In between the bands there is still a significant SC while the FC
80 is very small. The in-between band values of the SC decrease with increasing wavenumber, for 1140 cm^{-1}
81 they are $1.2 \times 10^{-22} \text{ cm}^2 \text{ molecule}^{-1} \text{ atm}^{-1}$ (46 times smaller than the in-band value), decrease by a factor of
82 15 at 2600 cm^{-1} and by a factor of 24 at 4770 cm^{-1} . The FC values in-between bands are below 6×10^{-26}
83 $\text{cm}^2 \text{ molecule}^{-1} \text{ atm}^{-1}$ and, thus, much smaller when compared to the SC for the in-between band position.
84 All values were taken from MT_CKD3.2 [Mlawer2019].

85 **1.2 Relevance of continuum for climate and remote sensing**

86 For atmospheric conditions for the case of the in-band continua for 1 atm total pressure (boundary layer
87 conditions) and 20 mbar H_2O , the FC optical depth is about 4 times larger than that of the SC. In contrast,
88 the impact of the FC in the atmospheric window region $800\text{-}1200 \text{ cm}^{-1}$ is small, while that of the SC is
89 significant for tropical conditions but negligible under subarctic winter conditions.

90 The climate impact of the continuum is twofold. While below 2000 cm^{-1} the OLR (outgoing longwave
91 radiation) is of importance, in the range $2000\text{-}10000 \text{ cm}^{-1}$ the absorption of solar radiation is relevant.
92 According to [Paynter2011] the OLR decrease due to the SC and FC for tropical condition is 8.4 and 2.7
93 W/m^2 , respectively. The solar radiation reaching the Earth's surface (in cloud-free skies), globally
94 averaged, is reduced by about 1.2 W/m^2 for the MT_CKD2.5 continuum model and 0.74 W/m^2 more for
95 the CAVIAR (Continuum Absorption in the Visible and Infrared and its Atmospheric Relevance)
96 continuum [Ptashnik2012]. These contribute a few % of components of the Earth's radiation balance.

97 The FC in the region 1300-2000 cm^{-1} is important since the region is used to derive water profiles from
98 nadir viewing satellite instruments utilized in numerical weather predictions [Newman2012]. Certainly,
99 the water continuum, and its role changing atmospheric transmittance or radiance, is of potential
100 importance for many remote sensing applications, both in-band and between-band, including
101 determination of cloud properties [Shine2012].

102 **1.3 Determination of continuum in the past**

103 The continuum is usually obtained from transmittance spectra (absorption coefficient spectra in the case
104 of CRDS (cavity ring down spectroscopy) measurements) by removing local line contributions calculated
105 typically from HITRAN line parameters (using the Voigt line shape). To avoid line parameter induced
106 errors only microwindows (troughs) between lines are used. This leads to large gaps in the derived
107 continuum in regions with many lines. Thus, this method unfortunately yields a relatively coarse
108 resolution, in particular for the in-band FC which is more susceptible to local line errors since at 1 bar the
109 water lines are 10 times wider than pure water lines at 20 mbar. A broadband determination of the FC
110 with low total pressure measurements gives a too weak continuum to be measured with usual
111 configurations of spectrometers like FTS (Fourier-Transform spectrometer).

112 **1.4 Previous measurements of H₂O near-IR continua**

113 Historically, many measurements of the SC and FC in the thermal infrared and microwave are available
114 [Mlawer2012,Mlawer2019,Shine2012,Shine2016]. Adjustments to these continua are still necessary
115 [Cormier 2005,Mlawer 2019], but it is generally quite well-characterized. This is not the case in the near-
116 IR (NIR), which is the focus here.

117 In-band continua from laboratory measurements have been reported for both the SC and FC, for various
118 NIR bands [Burch1985,Paynter2009,Ptashnik2004,Ptashnik2019]. These studies are in reasonable
119 agreement, but the dense line structure means that the continuum can only be obtained at certain
120 wavenumbers, and uncertainty in spectral line parameters is the dominant source of uncertainty
121 [Ptashnik 2019]. Nevertheless, these works indicate significant broad but distinct spectral features,
122 attributed to the water dimer, that are not represented in MT_CKD.

123 The between-band situation in the NIR is less clear. Most SC measurements are available in the 2500 cm^{-1}
124 ¹ between-band region [Shine2016,Richard2017]; at room temperature there is an order of magnitude
125 spread in the SC strength and disagreement in the temperature dependence. Many fewer measurements

126 are available at wavenumbers greater than 4000 cm^{-1} ; most reported SC and FC measurements are from
127 two laboratories using FTS (including those associated with the CAVIAR (Continuum Absorption in the
128 Visible and Infrared and its Atmospheric Relevance) project and Tomsk (who also report a measurement
129 using the photo-acoustic method [Kapitanov2018]) and one laboratory (Grenoble) using CRDS and
130 related cavity-laser techniques. Much of this work was reviewed in [Shine2016], with more recent
131 measurements reported by [Campargue2016,Richard2017,Lechevallier2018,Vasilchenko2019]. A general
132 problem with FTS measurements is the low sensitivity. In case of the weak in-between band signals the
133 stability of the instrument baseline becomes a severe source of uncertainty. For a given absorption path,
134 the intensity is limited by the vapor pressure which decreases with temperature. Lower temperatures,
135 significant for the atmosphere, can thus not be covered. Many of the cavity measurements have been
136 made near room temperature, with selected ones at higher temperature. There is currently a dearth of
137 measurements at lower temperatures. For the SC, the consistency between measurements and MT_CKD
138 varies with both temperature and wavenumber. In the $2.1\text{ }\mu\text{m}$ window the high-temperature FTS
139 measurements appear consistent the cavity-laser measurements, assuming a dimer-like temperature
140 dependence. This is not the case in the $1.6\text{ }\mu\text{m}$ window, with the cavity-laser measurements indicating a
141 smaller temperature dependence. One important possibility [Shine2016] is that the SC changes shape
142 with temperature, and thus there is no common temperature dependence for the SC at all between-
143 band wavenumbers, which is contrary to the representation in MT_CKD.

144 For the between-band FC, there is only one set of FTS measurements covering a significant wavenumber
145 range [Ptashnik2012] and a more limited set of cavity-laser measurements at selected wavenumbers
146 [Mondelain2015,Vasilchenko2019,Mondelain2020]. Although these measurements are not in full
147 agreement, they consistently indicate that the FC in the center of the windows is significantly higher than
148 MT_CKD. The derivation of FC from laboratory measurements is reliant on an accurate SC, but on the
149 other hand, the weaker temperature dependence means that observations at elevated temperatures are
150 likely more relevant to atmospheric conditions. Although no temperature dependence could be detected
151 within the measurement uncertainties in [Ptashnik2012] this does not rule out the possibility of a weak
152 dependence, as has been suggested in other spectral regions [Cormier2005].

153

154 1.5 Physical background of continuum

155 About half of the 3 μm in-band SC at room temperature (somewhat less for the 6 μm band) consists of
156 the spectrum of the bound H_2O dimer [Epifanov1997;Ptashnik2011; Serov2017;Ptashnik2019]. A second
157 component is the quasi-bound (metastable) dimer showing the spectrum of the extremely broadened
158 water monomer. Serov postulated a third term caused by middle wing deviations from the Voigt line
159 profile. This was necessary since the amount of stable and metastable dimers calculated from virial
160 coefficients represented by the total dimerization equilibrium constant K_{eq} was too small to model the
161 observed continuum. [Ptashnik2011;Ptashnik2019] tried to model the continuum without middle wing
162 contributions but also found disagreement with the equilibrium constant. The bound dimer spectrum
163 shows discrete bands differing from the monomer bands (see Figure 5 in [Ptashnik2011], Figure 5 in
164 [Ptashnik2019]). The different contributions to the SC together with the different bound dimer bands
165 cause a strong spectral dependence of the temperature dependence of the continuum. The amount of
166 bound dimer is significantly reduced with increased temperature due to dissociation. A spectrum of the
167 bound dimer can also be seen in the SC below 50 cm^{-1} [Odintsova2019]. Rotationally resolved structure
168 of dimer lines in gaseous water was found by [Serov2014] between 188 and 258 GHz. Ma et al. give
169 theoretical calculations of the SC and its temperature dependence using far wing impact theory alone
170 [Tipping1995, Ma2008]. Although the far wings cannot explain the entire SC because of the statements
171 above, a contribution of this type is still possible.

172 It should be mentioned that spectroscopic measurements of H_2O samples at atmospheric conditions are
173 not the favorite method to determine H_2O dimer spectroscopy, since only about 0.1% of the water at 20
174 mbar is bound dimer at 296K, as can be calculated from the dimerization equilibrium constant.
175 [Serov2017]. There is rather long history of spectroscopic investigations of the H_2O dimer in molecular
176 beams and matrix isolation spectroscopy, listed in review [Mukhopadhyay2015].

177 In contrast to the SC, the FC does not show strong in-between band contributions and is mostly
178 interpreted as far wing deviation from the Lorentz profile. A theoretical model is based on the impact
179 theory developed by Tipping and Ma [Tipping1995] covering SC and FC. Insights into far wings are
180 available from measurements and analysis of Ar-broadened HCl [Tran2017], which is a simple diatomic
181 molecules with lower line density than H_2O , thus line wings are visible farther away from the line center.
182 Super- and sub-Lorentzian contributions were modeled applying Classical Molecular Dynamics
183 Simulations (CMDS). While close to the band center super Lorentzian lineshape dominates, the high J
184 lines showed sub-Lorentzian behavior, which was attributed to line mixing.

185

186 2. Continuum determination

187 2.1 Method

188 Water measurements between 1800 and 4000 cm^{-1} with high quality line parameters already
189 determined [Loos2017;Loos2017a] allowed the prototyping of a new method for continuum
190 determination which is described here. The major advantage of the method is the use of the same
191 spectra to derive the spectroscopic line parameter database and the continuum information. Thus, the
192 occurrence of large spectral gaps and systematic errors due to local line errors present in previous work
193 can be avoided. This is especially an improvement for the in-band determination of the FC where a high
194 line density of local water lines is present.

195 The spectra are fitted within short microwindows with a multispectrum fitting approach utilizing the
196 Hartmann-Tran line profile [Tran2013;Tran2014] including Rosenkranz line mixing. Since also instrument
197 properties like the instrumental line shape were well characterized, the spectra could be fitted down to
198 the noise level. Since the input to the line fitting are transmittance spectra (which were obtained by
199 dividing sample spectra by empty cell spectra), the fitted baseline contains the continuum information.
200 The continuum is then retrieved from the baselines. It should be emphasized that systematic errors
201 would occur when only using the Voigt profile for analyzing the spectra since a) it would not be possible
202 to fit the spectra down to the noise level, which in turn would cause systematic errors in the fitted
203 baseline, and b) an effective Voigt fit of non-opaque laboratory spectra leads to systematically too small
204 Lorentz broadening parameters [Birk2016] due to speed dependence and Dicke narrowing which would
205 also introduce systematic errors in the fitted baselines. Furthermore, it should be mentioned that line
206 mixing influences the entire Lorentz profile including regions far away from the line center. Due to the
207 multispectrum approach utilizing both, opaque and non-opaque, spectra combined with the Hartmann-
208 Tran line profile and Rosenkranz line mixing lines with opaque centers can also be fitted and, thus, a
209 reliable baseline is available even in this case.

210 It should be noted that the measurements were primarily made to determine line parameters and not
211 the continuum. So neither the measurement plan nor the baseline stability was adapted to optimum
212 continuum determination. To use the fitted baselines to determine the continuum is only a step in
213 developing the simultaneous multispectrum fitting of continuum and line parameters. The results are
214 useful for the in-band region but not for the in-between bands regions.

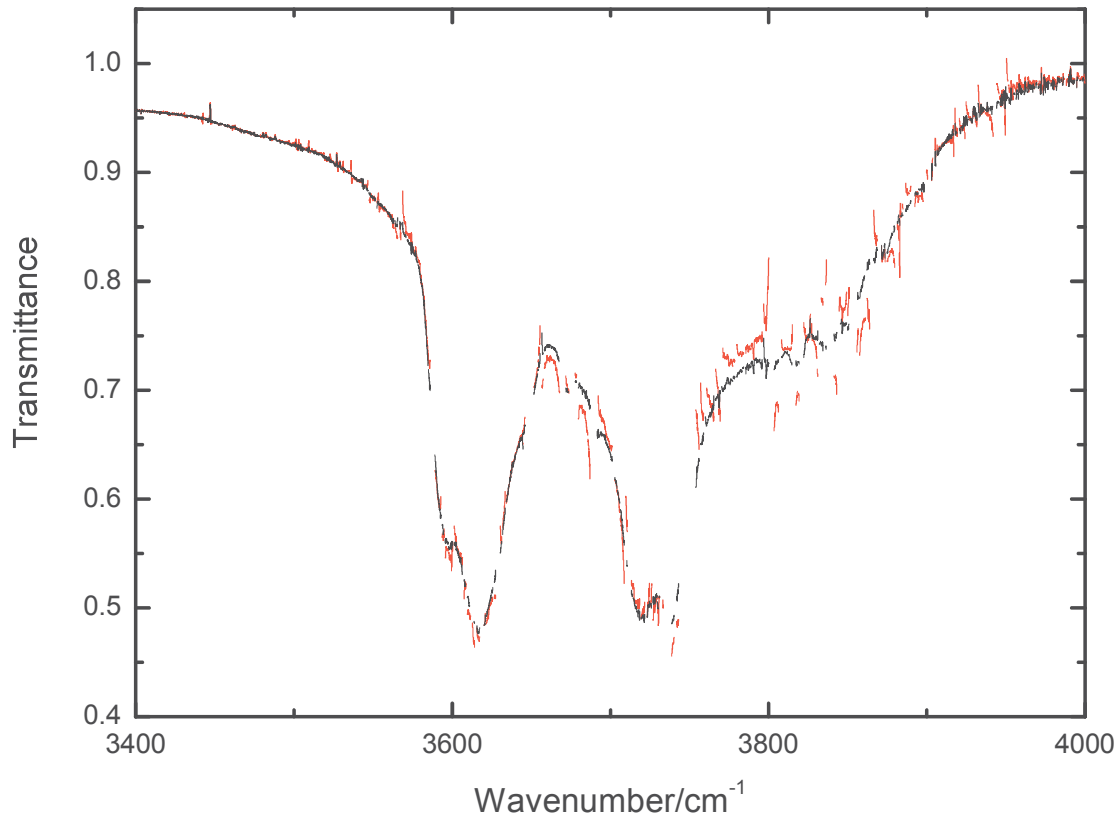
215 2.2 Data

216 In the previously mentioned publications of Loos et al. the details on the measurements and
217 instrumental setup are given. 15 pure water measurements and 24 air broadened measurements at 296
218 K, as well as 15 air broadened measurements at low or elevated temperature, 5 at 213 and 253 K and 10
219 at about 350 K, were recorded. The fitting was achieved in three steps: multispectrum fitting of the pure
220 water measurements was carried out first, then of the air broadened data and then of the data at low
221 and high temperatures. In each step, line parameters were determined and then kept fixed in the next
222 steps. For example, line positions and intensities as well as self broadening line profiles were fitted in the
223 first step and kept fixed in the following steps. In the case of pure water measurements, the spectrum
224 was cut in 0.25 cm^{-1} to 0.75 cm^{-1} sized microwindows and 0.5 cm^{-1} to 3 cm^{-1} in case of foreign
225 broadening. The line profiles were cut at $\pm 100 \text{ cm}^{-1}$ from their centers. Thus, all lines were considered
226 which are inside a distance of $\pm 100 \text{ cm}^{-1}$ from the microwindow boundaries. The final multispectrum
227 fitting is carried out with all line parameters in the final state to correctly account for the influence of the
228 updated lines in the $\pm 100 \text{ cm}^{-1}$ range. This guarantees that there is no local line influence on the baseline
229 and hence not on the continuum. A baseline quadratic in wavenumber is fitted for each microwindow
230 and each spectrum.

231 Initially, we tried to use the fitted baseline data to retrieve the continua. Unfortunately, it turned out
232 that there were some problems: a) In the case of self-broadened measurements there was line mixing
233 present which initially was rarely fitted, b) In some cases opaque regions covered most or all of a
234 microwindow and no baseline was available due to the small microwindow width.

235 Because of this, new microwindows were defined with substantially larger width ranging from 6 to 16
236 cm^{-1} . Microwindow boundaries were placed at points with minimum absorption. Larger microwindows
237 required to fit or refit line mixing in order to get residuals close to the noise level. Reaching the noise
238 level proves that the continuum does not have higher resolution than the microwindow widths. Since a
239 large microwindow covers several narrow microwindows of the original fit there are fewer baseline
240 parameters in the new fit than in the old fit. More baseline parameters defining smaller wavenumber
241 segments allow the incorporation of line profile information. The narrow quadratic polynomial baseline
242 segments can approximate line mixing while the wide baseline polynomials cannot. The width of the line
243 mixing contribution is too small for the wide baseline polynomials. If not considered, line mixing can fake
244 a high resolution continuum. Figure 1 shows the impact of the line mixing on the spectrum of
245 concatenated baselines of one of the measurements (case #4 in Table 1). The improvement of the
246 baseline quality and thus the derived continuum is considerable. The reason for the high importance of

247 self line mixing is the about 6 times larger self line mixing parameter when compared to air line mixing.

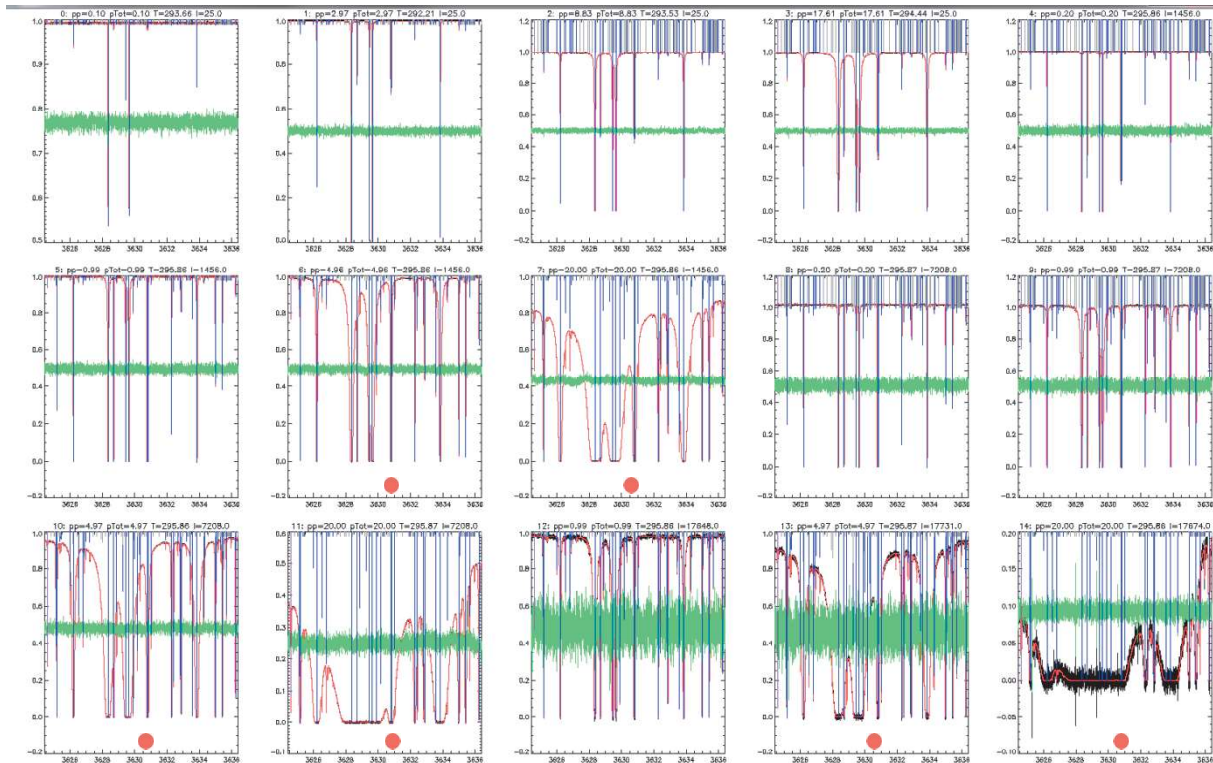


248
249
250
251 Figure 1. Concatenated fitted baselines from measurement #4, Table 1. Red: no line mixing or line mixing
252 from narrow microwindows, black: with line mixing from wide microwindows.

253
254 When line mixing was (re)fitted for a specific line, the Lorentzian width and the pressure induced line
255 shift were also refitted. Surprisingly, the air-broadened measurements did not require refitting the line
256 mixing already covered by [Loos2017,Loos2017a], who fitted more air line mixing parameters than self
257 line mixing parameters. Together with the initially somewhat wider microwindows for air-broadened
258 measurements this may be the reason that there was not so much line mixing hidden in the baseline
259 parameters. In the case of the self-broadened measurements line mixing had not been fitted in the

260 previous analysis. As stated above this can be attributed to the narrow microwindows which easily hide
 261 the line mixing effects in the quadratic baseline polynomial. The self broadening analysis applied
 262 narrower microwindows than the air broadening analysis due to the smaller pressure-broadened widths.
 263 The above mentioned microwindow boundary selection has the further advantage that baseline
 264 information is available close to both boundaries which enables interpolation of the baseline. For the air-
 265 broadened measurements, in several microwindows the central region was opaque and so did not have
 266 enough information to fit a quadratic baseline polynomial. Thus, the polynomial degree was limited to 1,
 267 which was applied to all microwindows. This was justified by verifying that the residuals of the
 268 multispectrum fit were still within the noise level. For the self-broadened measurements, the quadratic
 269 baseline was maintained. Figures 2 and 3 show examples of the multispectrum fit of pure H₂O and air-
 270 broadened measurements at room temperature. The measured spectra, the calculated spectra obtained
 271 from the fitted parameters (including baseline), and the residuals for the individual measurements can
 272 be seen. It can be seen that residuals are mostly within the noise level. After updating the spectroscopic
 273 database for the self-broadened line shape, the spectra were refitted with the narrow microwindows to
 274 ensure sufficient spectral resolution for the SC.

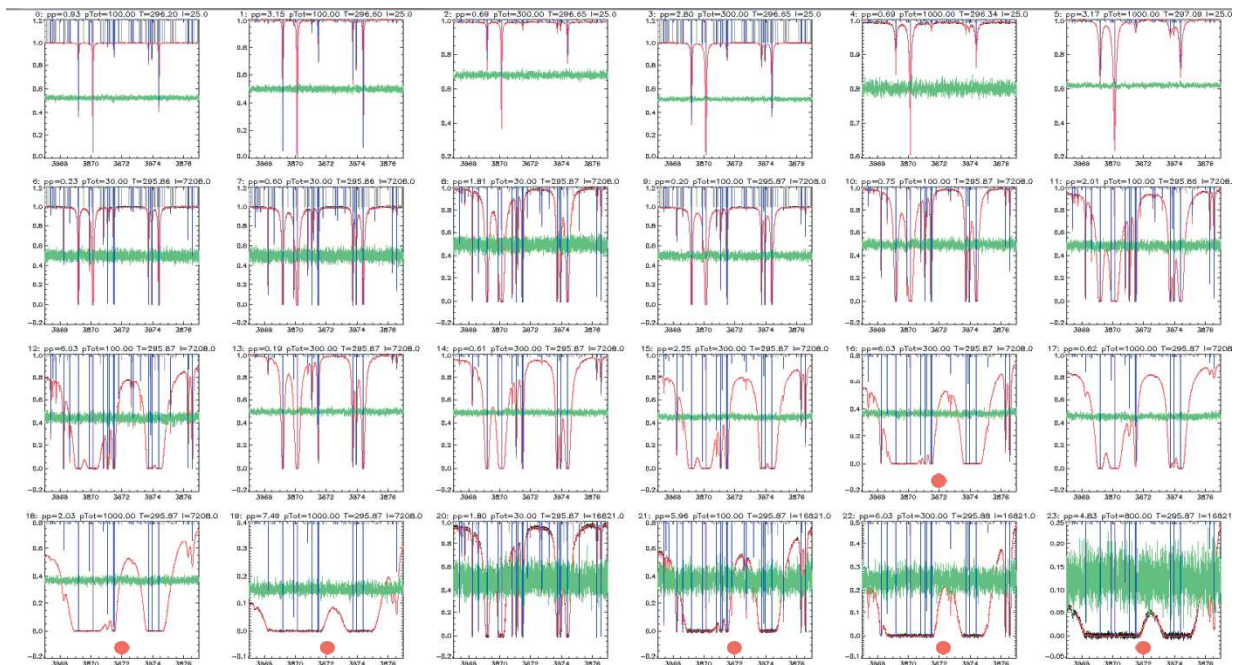
275
 276



277
 278 Figure 2. Screenshot of the multispectrum fit of the self broadening parameters in microwindow 3624.4-
 279 3636.4 cm⁻¹. Black: observed spectrum (mostly hidden beneath the red calculated spectrum), red:

280 calculated spectrum, green: (observed-calculated)x10 (shifted for better visibility), except last spectrum:
 281 (observed-calculated)x1, blue and grey: stick spectrum, stick length giving rough estimate of peak
 282 absorptance. Red dots indicate spectra/baselines used in the subsequent continuum fit. H₂O pressure
 283 [mbar], total pressure [mbar], temperature [K], and absorption path [cm] are noted above each graph
 284 and are listed in the same sequence in Table 2 in [Loos2017].

285



286

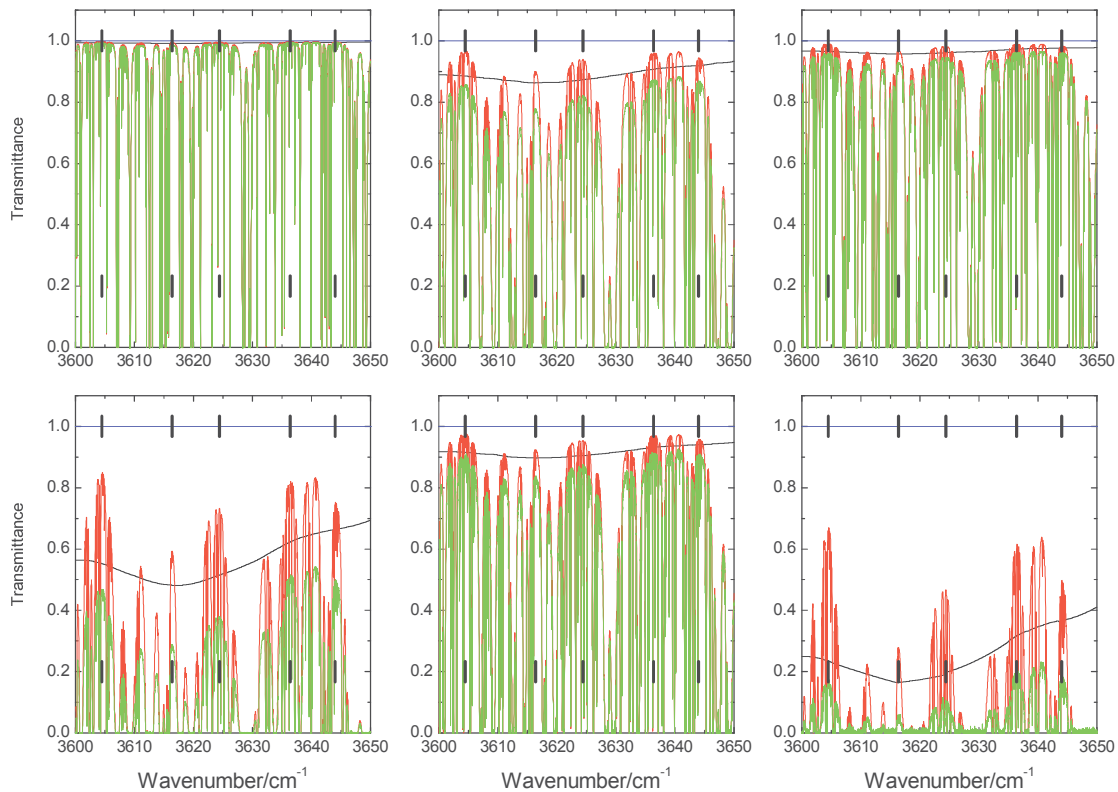
287 Figure 3. Screenshot of the multispectrum fit of the air broadening parameters in microwindow 3867-
 288 3877 cm⁻¹. Black: observed spectrum (mostly hidden beneath the red calculated spectrum), red:
 289 calculated spectrum, green: (observed-calculated)x10 (shifted for better visibility), blue and grey:
 290 stick spectrum, stick length giving rough estimate of peak absorptance. Red dots indicate spectra/baselines
 291 used in the subsequent continuum fit. H₂O pressure [mbar], total pressure [mbar], temperature [K], and
 292 absorption path [cm] are noted above each graph and are listed in the same sequence in Table 2 in
 293 [Loos2017a].

294

295 Figures 4 (self broadened) and 5 (air broadened) further illustrate the information flow from the spectra
 296 to the continua via the fitted baseline. The observed spectra are displayed as well as the modelled
 297 spectra from line parameters only, i.e. without continuum. Furthermore, the fitted baseline and the
 298 microwindow boundaries are shown. The visible red peaks contain the continuum information since the
 299 modelled spectra stand out from behind the observed ones at wavenumbers where continuum-induced

300 differences occur. It can be seen that most continuum information for the air-broadened measurements
 301 is close to the microwindow boundaries. In between, the baseline is linearly interpolated across the
 302 opaque regions which do not give any continuum/baseline information. The self-broadened data in
 303 Figure 4 shows more red than Figure 5 indicating more information due to the narrower lines and thus
 304 less extended opaque regions. The microwindow boundaries are not visible in the baselines in Figure 4
 305 while they appear in Figure 5. The less congested self-broadened spectra allowed the use of small
 306 microwindows with a quadratic baseline, while the air-broadened spectra only allowed large
 307 microwindows with a linear baseline. The discontinuities visible in Figure 5 indicate errors in the fitted
 308 baseline and/or errors due to the linear representation of the baseline. The gap in the final baseline
 309 spectrum is caused by a too opaque spectrum throughout the microwindow.

310

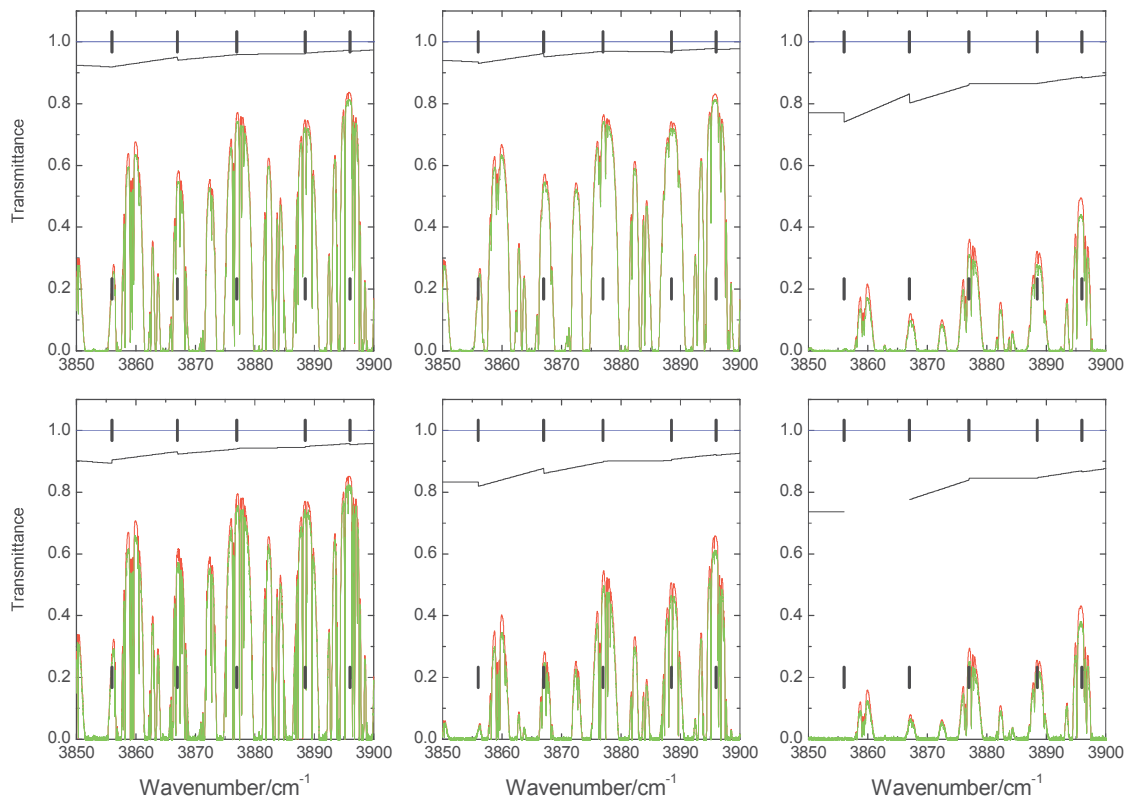


311

312 Figure 4. Transmittance contributions for SC determination from self-broadened spectra (Top left to
 313 bottom right: measurements 1-6 in Table 1). Green: observed spectra, red: modelled spectra from line

314 parameters only, black: fitted baselines, black sticks: microwindow boundaries, blue: 100%
315 transmittance.

316



317

318 Figure 5. Transmittance contributions for continuum determination from air-broadened spectra (Top left
319 to bottom right: measurements 7-12 in Table 1). Green: observed spectra, red: modelled spectra from
320 line parameters only, black: fitted baselines, black sticks: microwindow boundaries, blue: 100%
321 transmittance.

322

323 For the continuum analysis only spectra which have most information content regarding the continua
324 were considered. Table 1 lists the relevant measurement conditions for these spectra. The continuum
325 information content for each measurement, “ IC_s ” and “ IC_f ”, are also listed in the table. In case of the SC
326 we have $IC_s = p_{H_2O}^2 \times l$ and in case of the FC $IC_f = p_{H_2O} \times p_{tot} \times l$, where p denotes pressure and l the

327 absorption path. In addition to the information content it should also be taken into account that the FC
 328 according to MT_CKD (see above) is 12 times weaker. In the case of the SC and the pure H₂O
 329 measurements, it can be seen that two measurements (#4 and #6) are dominating the continuum
 330 information. In the case of the air-broadened measurements the information content for the SC is about
 331 10 times smaller. The high temperature measurements have substantially less information and the
 332 disadvantage that SC and FC have to be fitted simultaneously.

333 Table 1: Measurements for continuum analysis. The list contains H₂O pressure, total pressure, absorption
 334 path, SC information content (IC_s), FC information content (IC_f), and baseline scaling correction factors
 335 (see section "Continuum fits"). The first block are pure H₂O measurements at 296 K, the second air-
 336 broadened measurements at 296 K and the third air-broadened measurements at 353 K.

#	p _{H₂O} /mbar	p _{tot} /mbar	l/m	IC _s	IC _f	basecorrfact
1	4.9626	4.9626	14.50	350		1.001
2	20.0	20.0	14.50	5800		1
3	4.9651	4.9651	72.08	1773		1
4	20.0	20.0	72.08	28800		1
5	4.9655	4.9655	177.3	4354		0.994
6	20.0	20.0	176.7	70680		1
7	6.0	300	72.08	2592	129600	0.999
8	2.0	1000	72.08	288	144000	1
9	7.5	1000	72.08	4050	540000	1.005
10	6.0	100	168.21	6048	100800	1.001
11	6.0	300	168.21	6048	302400	1.003
12	4.8	800	168.21	3870	645000	1.002
13	0.6	100	72.08	26	4325	1.001
14	2.0	100	72.08	288	14416	1.002
15	5.7	100	72.08	2342	41086	1
16	17.3	100	72.08	21570	124700	1
17	0.6	100	168.21	61	10093	1.003
18	2.0	100	168.21	673	33642	1.004
19	6.0	100	168.21	6056	100926	1

337 2.3 Fitting procedure

338 The original transmittance spectra were inspected to assess the accuracy of the 100% level. The 100%
 339 baseline initially was not considered a relevant issue for the line parameter retrieval and the baseline
 340 polynomial coefficients contain the baseline fluctuations. Around 2600 cm⁻¹ there were only few lines
 341 and the continuum was expected to have a contribution to the baseline of 0.2% (calculated from

342 MT_CKD3.2) for the largest information content for the SC. Thus, this region was assigned to 100% and
343 the baseline coefficients were corrected accordingly.

344 It turned out that for the self-broadened measurements the baseline was nicely horizontal, thus for most
345 measurements the 100% reference was useful for the 3400-4000 cm^{-1} region. In the case of air-
346 broadened measurements, where the pressure was much larger than in case of the self-broadened
347 measurements, the empty cell reference spectra were less valid. In this situation the baseline was bent
348 for most measurements and the 100% reference was only useful for few measurements. Furthermore,
349 the optical filter limits the range to 4000 cm^{-1} and the signal dropped substantially from 3900 to 4000
350 cm^{-1} leading to baseline problems in this region. Thus, the fitted continuum is not valid above 3900 cm^{-1} .

351 Software was developed to fit continua to the baselines. The scaled baseline segments were calculated
352 from the second/first order polynomials on a 0.01 cm^{-1} grid. The baseline uncertainty was inferred from
353 the statistical uncertainty of the 0th order baseline coefficient as determined from multispectrum fitting.
354 The model functions for pure water and foreign broadened measurements are given in the following
355 equations:

$$356 \quad t_{base} = \exp\left[-l \cdot (p_{H_2O})^2 \cdot F \cdot C_s\right]$$

$$357 \quad t_{base} = \exp\left[-l \cdot (p_{H_2O})^2 \cdot F \cdot C_s - l \cdot p_{H_2O} \cdot p_{air} \cdot F \cdot C_f\right]$$

358 with t_{base} the baseline, l the absorption path in cm, p_{H_2O} the water pressure in atm, p_{air} the air pressure in
359 atm, F the conversion factor from pressure to number density @296 K ($2.479 \times 10^{19} \text{ molec cm}^{-3} \text{ atm}^{-1}$), and
360 C_s and C_f the self- and foreign-continuum coefficients in $\text{cm}^2 \text{ molec}^{-1} \text{ atm}^{-1}$, respectively. The baselines of
361 all relevant spectra were fitted simultaneously. These models ensure the quadratic p_{H_2O} dependence of
362 the SC absorption and the $p_{H_2O} \cdot p_{air}$ dependence of the FC absorption. No systematic deviations from
363 these models were observed.

364 **2.4 Continuum fits**

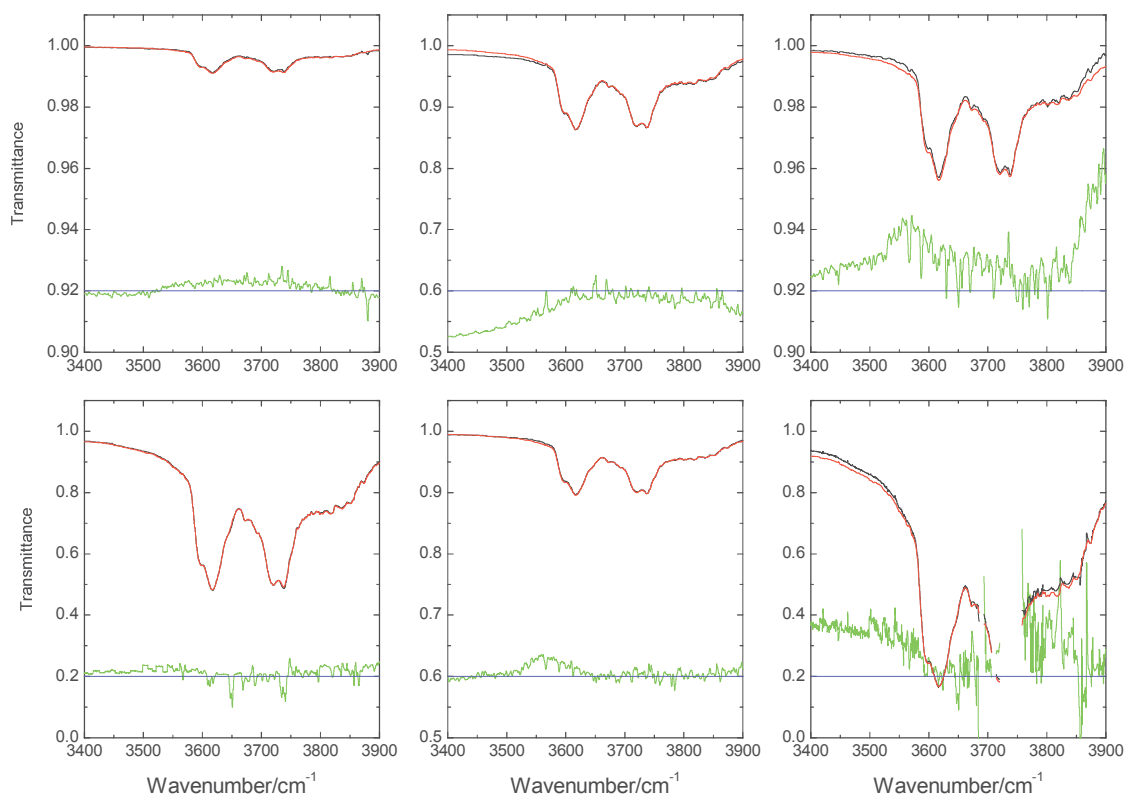
365 Three different fits have been performed.

366 *Self-continuum from pure H₂O measurements*

367 As described above the same narrow microwindows as in the original multispectrum fitting were used
368 after improving the line parameter database to obtain narrow second order polynomial baseline

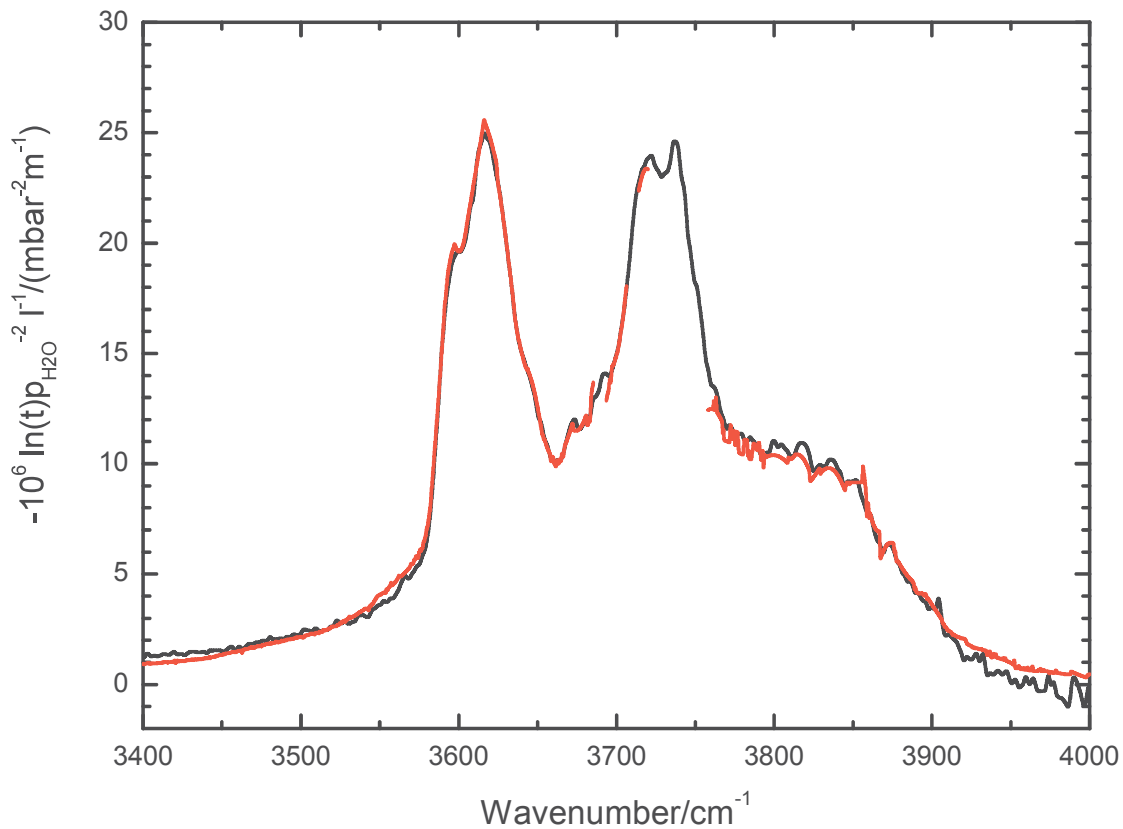
369 segments. Due to their high opacity, some baseline segments could not be fitted for some spectra
370 leading to gaps. As described above large microwindows have less gaps and thus baselines of the large
371 microwindows were used to fill the gaps. The final baselines appear noisy and were smoothed with a
372 Gauss function of FWHM of 2.4 cm^{-1} except for the measurement with largest information content which
373 still has gaps and the Gauss smoothing would decrease the available data substantially (convolution
374 shortens available ranges by a half-kernel width). The kernel FWHM for this measurement was reduced
375 to 0.5 cm^{-1} . Baseline correction scaling factors were applied to the observed baselines to reduce
376 residuals in the region with most continuum information. The correction values are listed in Table 1. Only
377 one measurement has a significant factor, but it is still well within 1% of unity. Observed and calculated
378 transmittances are shown in Figure 6 together with the residuals. Beside the measurement #6 with
379 maximum information content residuals are within 1%. The shapes of the residuals show baseline
380 problems. The residuals show no specific dependence on pressure or absorption path and thus indicate
381 the validity of fit model and input data. A further proof is the linear dependence of the optical depth on
382 $p_{\text{H}_2\text{O}}^2$. From the three pairs with the same pressures (see Table 1) the pair with the maximum absorption
383 path and thus maximum information content was selected and $-\ln(t)/(p_{\text{H}_2\text{O}}^2)$ formed. Figure 7 shows the
384 good agreement between the 5 and 20 mbar measurements (#5 and #6 in Table 1) where $p_{\text{H}_2\text{O}}^2$ differs by
385 the considerable factor 16. The final result of the SC fit is shown in Figure 9.

386



387

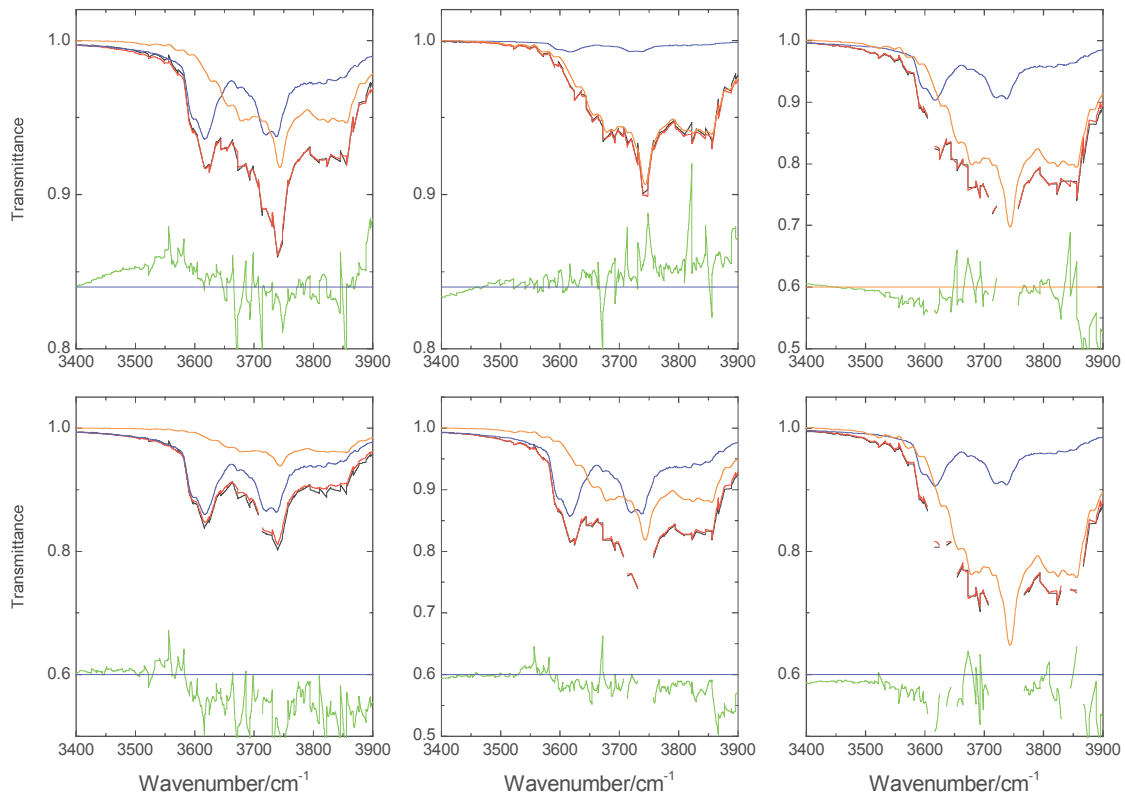
388 Figure 6. SC fit from pure H₂O measurements (from top left to bottom right measurements 1 to 6 in
 389 Table 1). Black: corrected observed baselines, red: calculated baselines, green: (observed-calculated) x
 390 10, blue: zero line for green trace. Note the different transmittance scales among the plots.



391
 392 Figure 7. Validation of $p_{\text{H}_2\text{O}}^2$ dependence of baseline optical depth. Black: 5 mbar, #5, red: 20 mbar, #6.

393
 394 *Foreign-continuum*

395 In the FC case only wide microwindows were used as described above. The SC was inferred from the fit
 396 described in the last section and used to calculate its contribution in the transmittance spectra. As in the
 397 SC, baseline correction scaling factors were introduced to reduce residuals in the region with most
 398 continuum information. The correction values are listed in Table 1. In contrast to the SC case, only one
 399 measurement required no correction factor. Again, all factors are well within 1%. Observed and
 400 calculated transmittances are shown in Figure 8 together with the residuals. In addition, the contribution
 401 of SC and FC to the transmittance is shown. Although the FC is generally much larger than the SC, the SC
 402 still makes a substantial contribution and is the dominant contributor at some wavenumbers.



405

406 Figure 8. FC fit. Black: corrected observed baselines (from top left to bottom right measurements 7 to 12
 407 in Table 1), red: calculated baselines, green: (observed-calculated) x 10, blue: transmittance of SC,
 408 orange: transmittance of FC, horizontal blue line: zero line for green trace. Note the different
 409 transmittance scales among the plots.

410

411 *Fit of high temperature SC and FC*

412 Unfortunately, there are no pure H₂O measurements at high temperature and furthermore, the
 413 maximum total pressure is 100 mbar only. Thus, it is not surprising that the information content of the
 414 continua (see Table 1) is much lower than for the room temperature measurements. SC and FC had to be
 415 fitted simultaneously. Due to the bad data quality uncertainties were not calculated.

416

417 3. Continua and error considerations

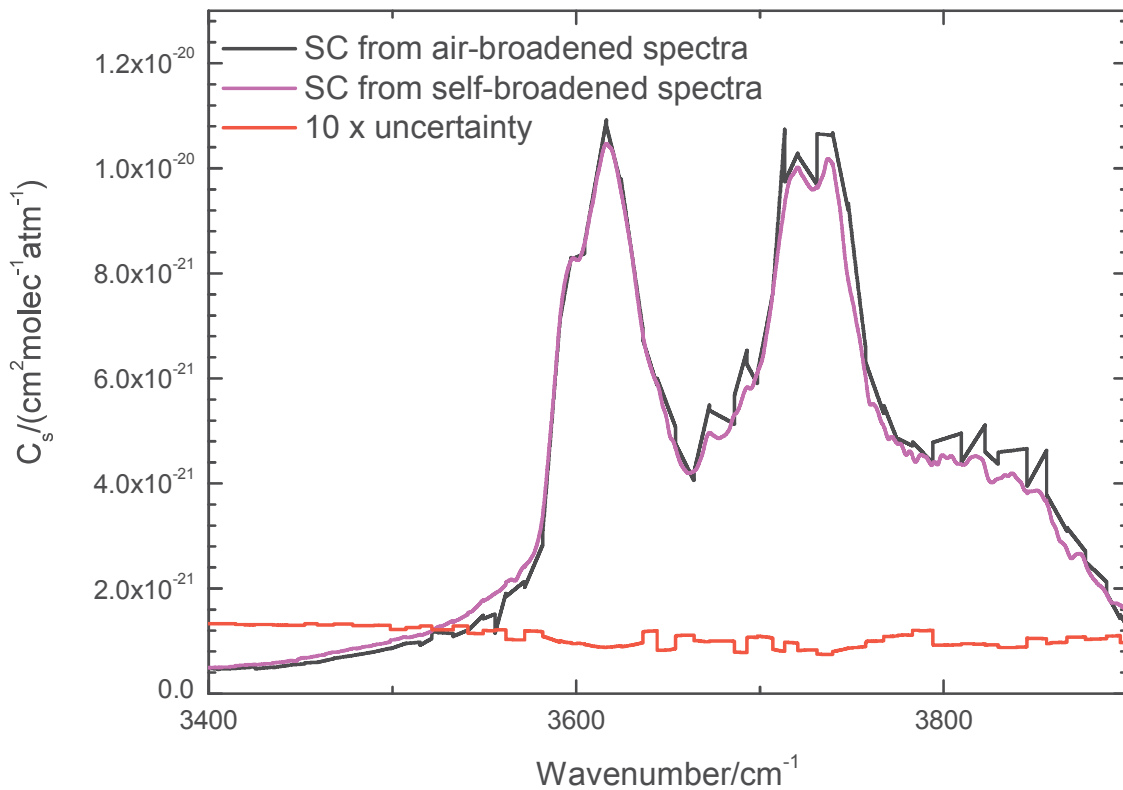
418 3.1 Self-continuum

419 As a consistency check, the self-continuum was also fitted using the air-broadened measurements only.
420 The continua obtained from pure water measurements only and from air-broadened measurements only
421 at 296 K are shown in Figure 9. The agreement is very good, showing that no additional errors are
422 present. As expected, the SC retrieved from air-broadened measurements only is a bit noisy, also the
423 spectral resolution is less since it is only based on the large microwindows. It can be seen that the SC is
424 rather smooth without resolved structure although its resolution is rather high with a FWHM of mostly
425 2.4 cm^{-1} . The maximum relative change, which may be linked to a resolved structure, is around 3820 cm^{-1}
426 and has an amplitude of 5%. Of course, this structure may be a result of the analysis and not real.

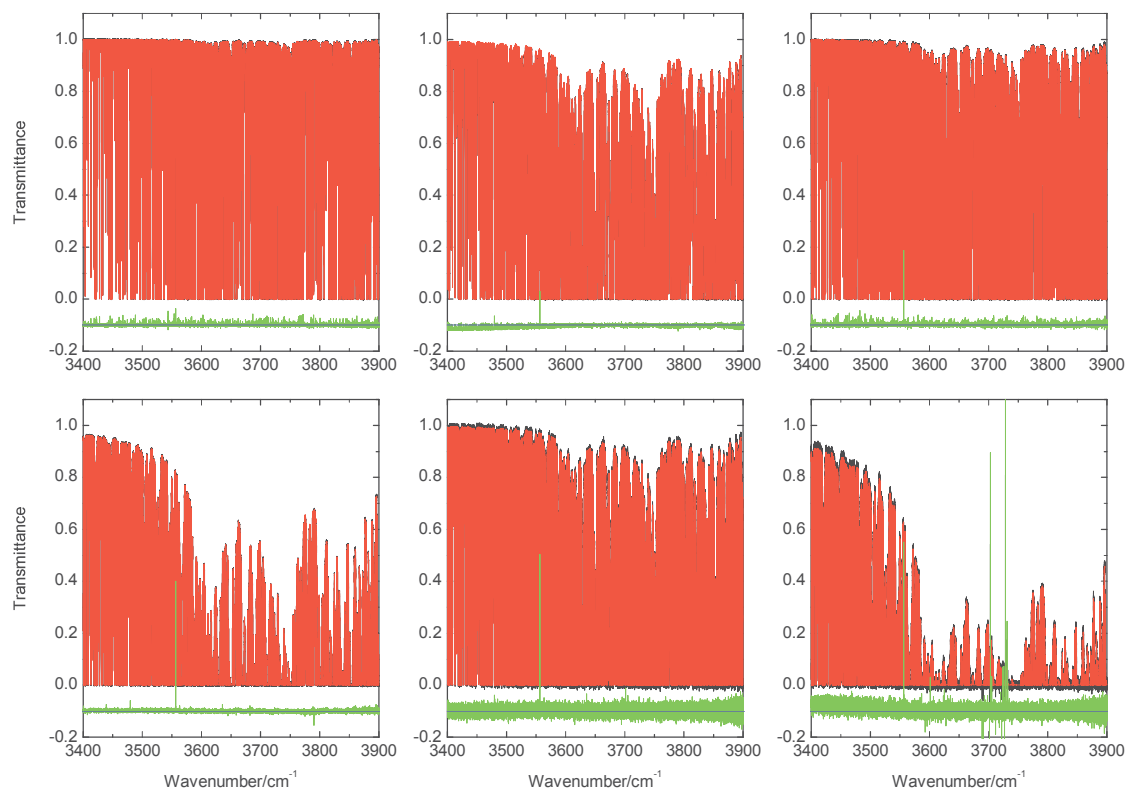
427 The largest error source for the continuum is the quality of the baseline. It was reported above that the
428 baseline quality of the pure H_2O measurements was rather good and only two out of six baselines had to
429 be scaled by factors deviating from unity by 0.1% and 0.6%, respectively. As a worst case it was assumed
430 that the baseline knowledge is <1%. The baseline of measurement 4 was scaled by 0.99 and all other
431 measurements were scaled to have similar residuals as in Figure 6. The fitted continuum was subtracted
432 from the original one and the difference gives the uncertainty displayed in Figure 9. This method
433 provides correlated errors only. The statistical uncertainties of the baselines yield an error <1% for the
434 continuum. It was stated above that the maximum amplitude of structures with respect to the smoothed
435 continuum is about 5%. A maximum relative error of this magnitude cannot be excluded. As a further
436 quality check, residuals are calculated from the scaled measured transmittance spectra and modelled
437 spectra calculated from the line parameters and the continuum, both derived from fitting. A first
438 impression is given in Figure 10. The instrumental line shape was not included in the modelled spectra
439 since the influence on the measured spectra is rather small. Furthermore, the calculation was carried out
440 on a 0.01 cm^{-1} grid, which is much coarser than that of the original measurements. The residuals appear
441 to be mostly noise beside a few spikes. These spikes were already in the measured transmittance
442 spectra. There were contaminant lines in the measured data which were removed by fitting the
443 contaminant spectra, calculating a transmittance and dividing the measured spectra by the calculated
444 transmittance spectra. When the contaminant spectrum has zero transmittance, spikes occur from
445 division of zero by zero. Details can be found in [Loos2017a]. The residuals of a smaller interval and - for
446 intercomparison - the residuals of the multispectrum fitting are shown in Figure 11. Whereas the
447 multispectrum fitting shows no residuals outside the noise level, there are some tiny residuals in the

448 calculation with the continuum. This is caused by the residuals in the continuum fitting (see Figure 6)
449 together with the smoothing. However, these residuals are so small that the effect on the continuum is
450 within the specified uncertainties and does not introduce additional systematic errors. These spectrally
451 medium resolved residuals (features of about 1-2 cm^{-1} width, see Figure 11) should vanish when the
452 multispectrum fitting is altered to fit continuum and line parameters simultaneously. Certainly, baseline
453 errors will cause residuals in this fit but usually much wider.

454 The important conclusion is that, with the continuum and the line parameters determined from the
455 same spectra, these spectra can be modeled close to the noise level. This also proves for the first time
456 that the ν_1/ν_3 in-band SC is almost smooth at 2.4 cm^{-1} resolution. There are still high resolution features
457 on the order of 5% of the local continuum value visible in the magenta curve in Figure 9, which we
458 cannot distinguish from noise or artefacts.



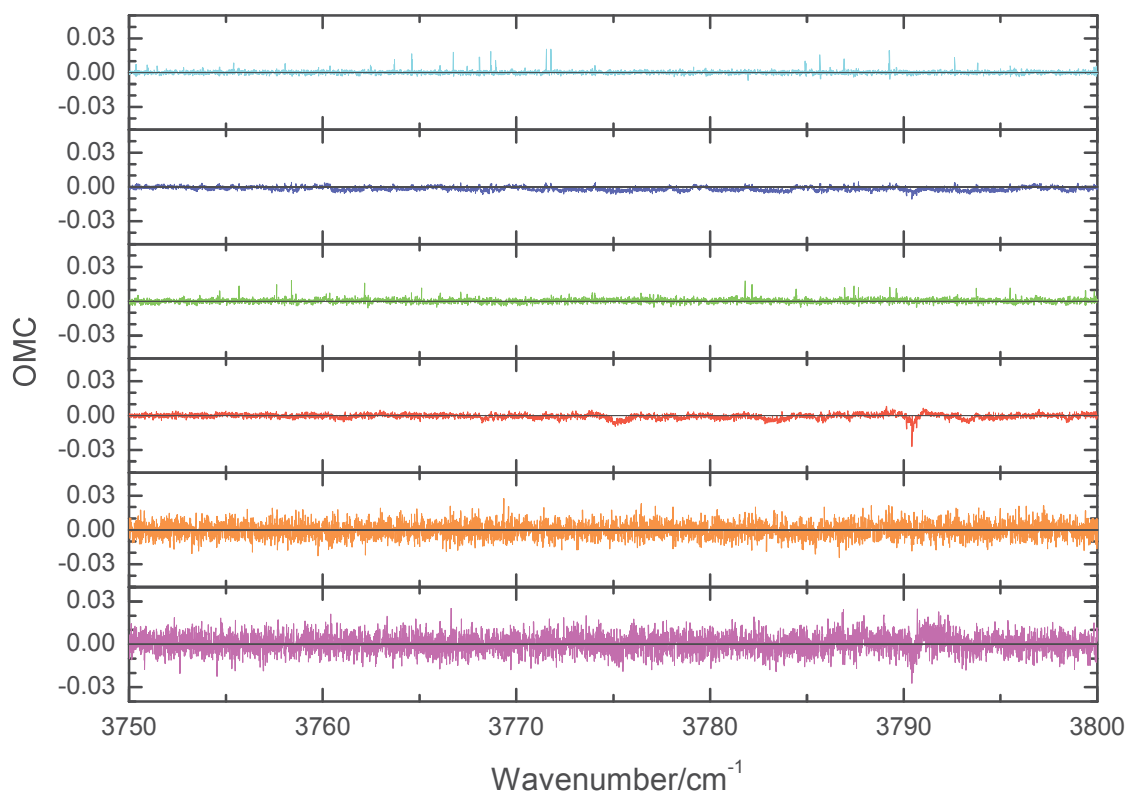
459
460 Figure 9. Fitted in-band SC from different measurements together with uncertainty for SC from self-
461 broadened spectra.



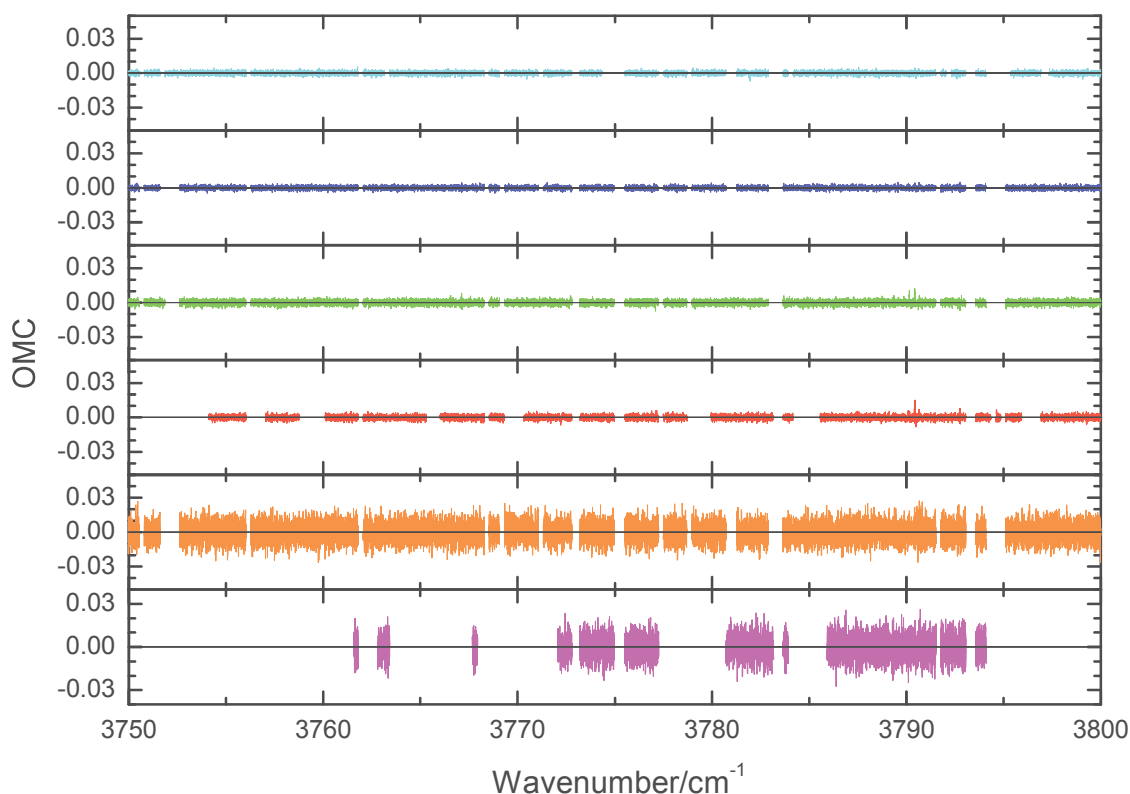
463

464 Figure 10. Measured spectra (from top left to bottom right measurements 1 to 6 in Table 1) and
 465 calculated spectra from fitted line parameters and SC. Black: measured spectra, red: calculated spectra,
 466 green: residuals (measured-calculated) x 2. Blue: zero line for green trace. For the spikes see text.

467



468



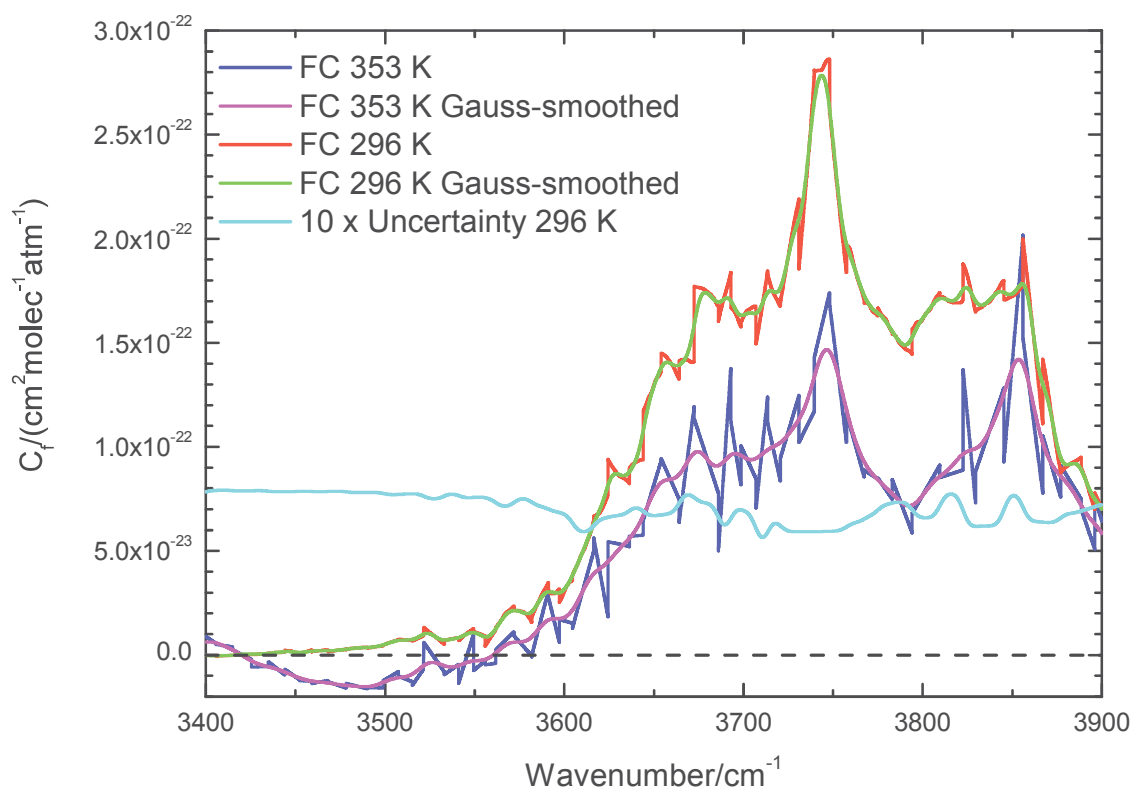
469 Figure 11. Top: excerpt of residuals (observed-calculated, OMC) from Figure 10, bottom: multispectrum
 470 fit residuals. Traces from top to bottom in each graph correspond to measurements 1 to 6 in Table 1.
 471 Note that the noise on top and bottom appears different due to the different point spacing (see text).
 472 Gaps in the bottom traces indicate that the corresponding spectrum was not included in the initial
 473 multispectrum fit. Non-noise residuals in the top graph show resolution of 1-2 cm^{-1} and amplitudes $<1\%$.
 474 The spikes in 1st and 3rd trace top originate from the missing instrumental line shape in the model.
 475

476 3.2 Foreign-continuum

477 The FC is shown in Figure 12. In contrast to the SC the analysis was carried out with baselines obtained
 478 from multispectrum fit with wide microwindows, as stated above. The wide linear baseline segments
 479 cause zigzag structures in the fitted continuum. Thus, Gauss smoothing was applied selecting σ as small
 480 as possible in order to remove the discontinuities. The selected Gauss FWHM of 7.2 cm^{-1} (corresponding
 481 to a Gauss σ of 3 cm^{-1}) was applied, and the results are also shown in Figure 12. The results for 353 K are
 482 shown for completeness, but due to the insufficient data (only foreign broadened measurements with
 483 single air pressure 100 mbar, see Table 1) the difference to 296 K may not be real, as can be seen from

484 the negative values around 3500 cm^{-1} . The error analysis was performed as described for the SC. The
485 baseline of measurement 9 was scaled by 0.99 and all other measurements were scaled to have similar
486 residuals as in Figure 8. The error is also displayed in Figure 12. The statistical error was $<2\%$ for most of
487 the region $3600\text{-}3900\text{ cm}^{-1}$. Residuals for the smoothed continuum were calculated for baselines and
488 compared to the original residuals in Figure 8. For some spectra in some spectral regions, the residuals
489 were increased which is not surprising since the original unsmoothed continuum from the fit should yield
490 the optimal residuals.

491 As stated above, the microwindows were selected to have transmittance maxima at their borders,
492 resulting in microwindow widths varying between 6 and 16 cm^{-1} . Certainly, this selection has an influence
493 on the retrieved continuum. Alternative microwindow borders were chosen for the region $3800\text{-}3900$
494 cm^{-1} still trying to use transmittance maxima as borders. The new borders were positioned
495 approximately in the center of the old microwindows. Continuum fits were performed and the residuals
496 were much larger than before. Clearly linear baselines work best when the borders are at transmittance
497 maxima since then the linear interpolated baseline is feasible. The alternative microwindows mostly had
498 lower transmittances at the borders and the linear baseline is less well determined. The fitted continuum
499 showed more structure and had a maximum disagreement with the original one of 15% in a local region
500 of 10 cm^{-1} . It is hard to specify an error on the relative continuum, i.e. how much structure is real, or
501 whether the continuum is smooth. An estimated error of 15% is definitely too large and, given the
502 differences of smoothed and unsmoothed continuum, 4% (average uncertainty given in Figure 12) is too
503 small. Thus 10% is assumed as an approximate number.

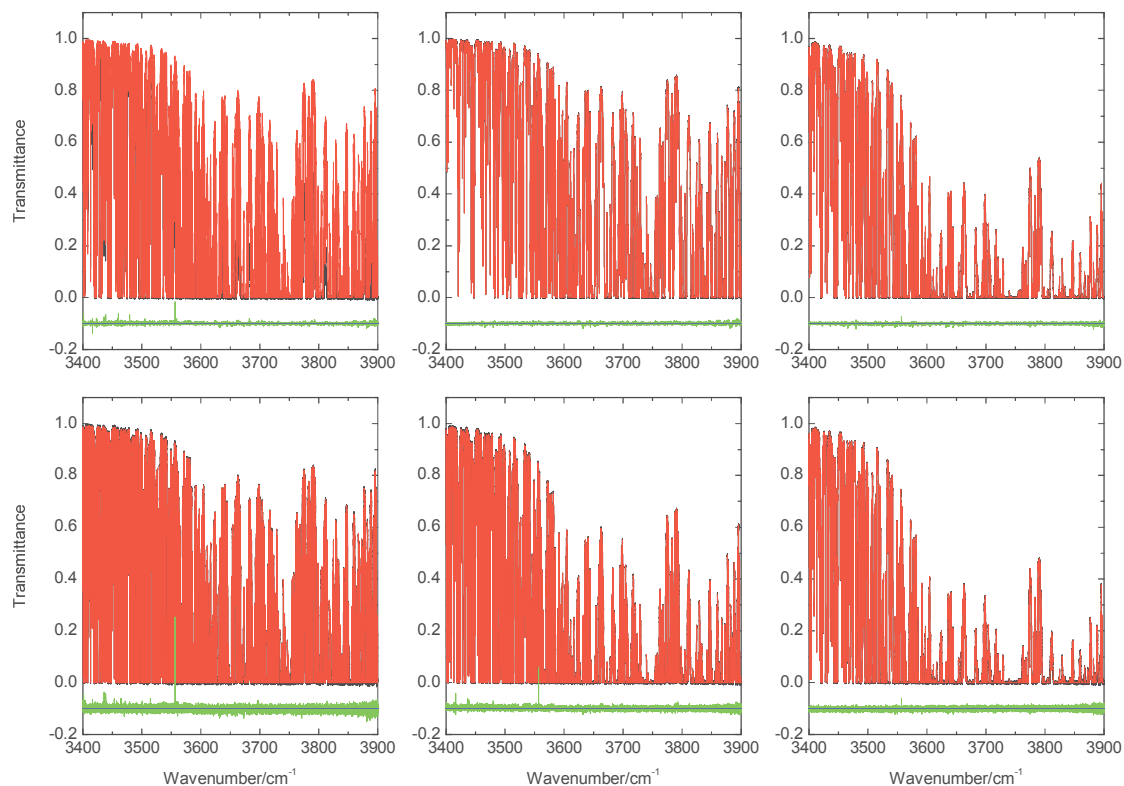


504
 505 Figure 12. Foreign continua smoothed and unsmoothed at 296 K and 353 K together with uncertainty of
 506 296 K continuum from baseline errors.

507 As in case of the SC, as a further quality check, residuals are calculated from the scaled measured
 508 transmittance spectra and modelled spectra calculated from the line parameters and the continuum. A
 509 first impression is given in Figure 13. Spikes are due to the missing ILS or due to opaque lines from
 510 contaminants as already explained for SC. Besides the spikes, the residuals look satisfactory. A more
 511 detailed view is given in Fig 14. In contrast to the SC where residuals of the multispectrum fitting are
 512 noise, in case of the FC small residuals outside the noise are present. The modelled spectra using the
 513 continuum show similar sized residuals as the multispectrum fitting. The unsmoothed continuum
 514 produces similar residuals. Again, as in case of SC, when continuum and line parameters were
 515 determined from the same spectra these spectra can be modeled close to the noise level. The inferred
 516 self-continuum also did not cause residuals, which was expected due to the good agreement shown in
 517 Figure 9. Note that the SC makes a substantial contribution to the air-broadened measurements as can
 518 be seen Figure 8.

519 The 296 K SC and FC together with the uncertainties can be found in the supplementary material.

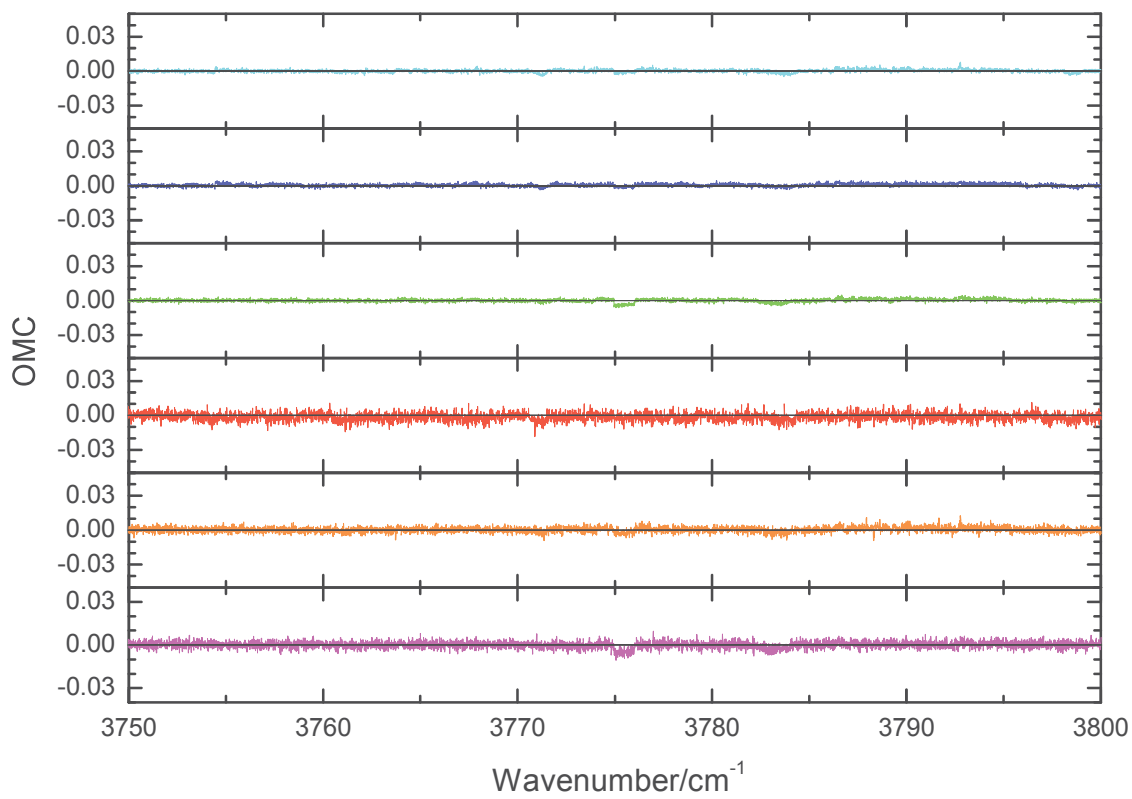
520



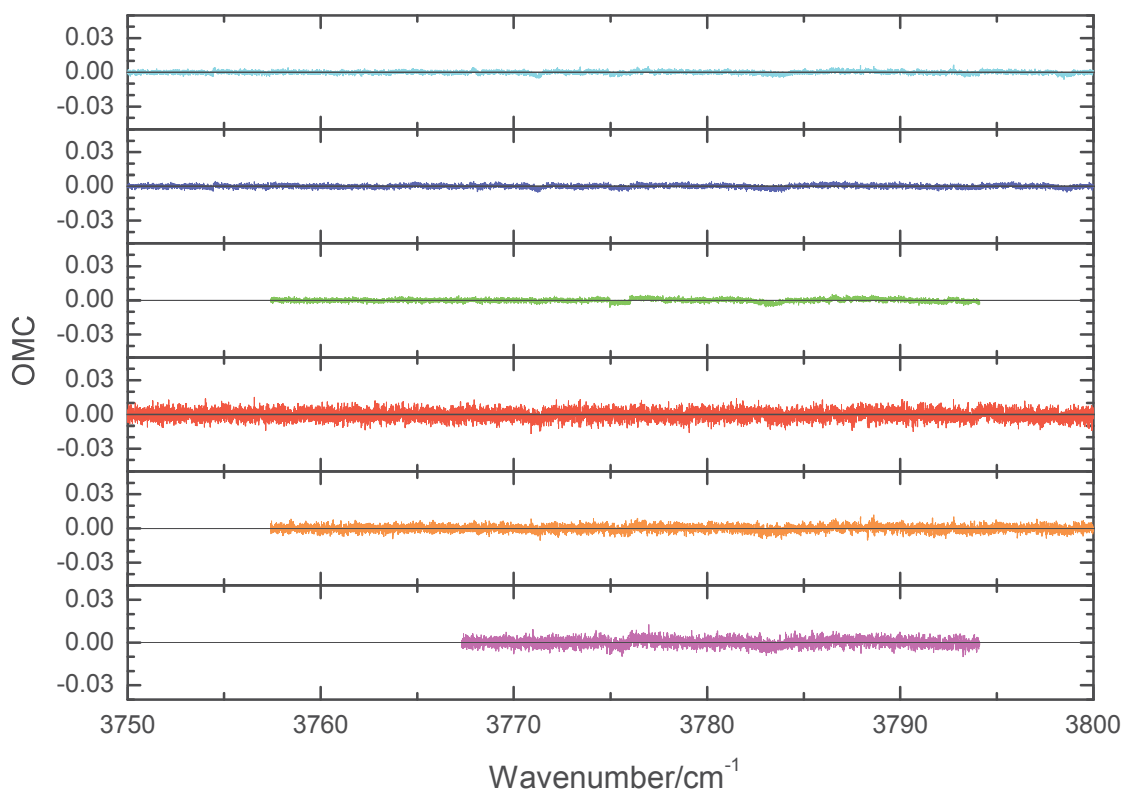
521

522 Figure 13. Measured spectra (from top left to bottom right measurements 7 to 12 in Table 1) and
523 calculated spectra from fitted line parameters, FC, and SC. Black: measured spectra, red: calculated
524 spectra, green: residuals (measured-calculated) x 2. Blue: zero line for green trace. For the green spikes
525 see text.

526



527



528
 529 Figure 14. Top: excerpt of residuals (observed-calculated, OMC) from Figure 10, bottom: multispectrum
 530 fit residuals. Traces from top to bottom of each graph correspond to measurements 7 to 12 in Table 1.
 531 Note that the noise on top and bottom graphs appears different due to the different point spacing (see
 532 text). Gaps in the bottom traces indicate that the corresponding spectrum was not included in the initial
 533 multispectrum fit.

534 4. Analysis of self-continuum

535 4.1 Shape of bound dimer bands

536 The positions and intensities of the H₂O dimer fundamentals have been studied in *ab initio*, e.g.
 537 [Kjaergaard2008] and experimental work, e.g. [Ceponkus2008,Kujanov-Prozument2010]. In the 3 μ m
 538 region there are four fundamentals. Forming averages among the cited studies shows that the positions
 539 and intensities of the three stronger fundamentals agree within ± 20 cm⁻¹ and $\pm 20\%$ (1σ), respectively.

540 [Ptashnik2011] simulated the dimer spectrum based on VPT2 in [Kjaergaard2008] assuming the dimer
541 bands to be simple Voigt profiles with 60 cm^{-1} FWHM, which is a very approximate estimate of a band
542 envelope. In [Ptashnik2019] most of the fundamentals were taken from [Kujanov-Prozument2010] and
543 two fundamentals shifted to better match the observed continuum. In an older *ab initio* work [Tso1998]
544 calculated the rovibrational spectrum of the dimer between 0 and 20000 cm^{-1} . We found too large
545 differences to the observed continuum to use the results in this investigation.

546 In the following the expected rovibrational spectrum of the H_2O dimer in the $3\text{ }\mu\text{m}$ region will be
547 discussed. The B and C rotational constants are about equal, approximately 0.2 cm^{-1} and the A rotational
548 constant is about 7 cm^{-1} [Mukhopadhyay2015]. The H_2O dimer is a nearly prolate top molecule. Because
549 of the much higher moment of inertia, the rotational constants are significantly smaller when compared
550 to the monomer with $C\approx 9\text{ cm}^{-1}$, $B\approx 15\text{ cm}^{-1}$, $A\approx 28\text{ cm}^{-1}$. This difference has a large impact on the shape of
551 the dimer bands when compared to the monomer bands. There are three strong rovibrational bands in
552 the $3\text{ }\mu\text{m}$ region. The band around 3597 cm^{-1} is the dimer fundamental ν_3 which corresponds to the
553 symmetric OH stretch of the donor H_2O [Kjaergaard2008]. The axis with the smallest moment of inertia
554 (A-axis) is nearly parallel to the H-bridge OH donor bond and close to both O atoms. The donor
555 symmetric OH stretch changes the dipole moment both parallel and perpendicular to the A-axis and
556 therefore the rotational structure should show both the parallel and perpendicular band of a prolate
557 symmetric top molecule (see [Herzberg1945], Fig 122 and Fig 128, respectively). For the dimer
558 fundamental ν_1 , corresponding to the ν_3 of the donor H_2O around 3730 cm^{-1} , the vibration changes also
559 both the dipole moment parallel and perpendicular to the A-axis. In contrast to this the ν_9 around 3749
560 cm^{-1} (antisymmetric OH stretch of the acceptor H_2O) changes the dipole moment only perpendicular to
561 the A-axis. Rotationally resolved $\Delta K_a=1$ transitions in the ν_9 were observed by [Huang1988,Huang1989]
562 confirming the perpendicular band type. It should be mentioned that the rovibrational band types were
563 also derived in [Huang1989]. In contrast to [Kjaergaard2008] the donor symmetric and asymmetric O-H
564 stretches were treated as localized “bonded” and “free” O-H stretches, respectively. This would lead to
565 almost parallel and perpendicular bands, respectively. As shown later, both bands have about similar
566 parallel and perpendicular contributions, more in line with the vibrational modes as described by
567 [Kjaergaard2008]. Furthermore, in [Huang1989] the “bonded” O-H stretch has a band center at 3545 cm^{-1}
568 1 which is in contradiction to [Kjaergaard2008].

569 Due to the five low lying fundamentals only 14% of the $3\text{ }\mu\text{m}$ vibrational bands originate from the ground
570 state. The rest is distributed among about 20 hot bands, with different rotational and centrifugal

571 distortion constants and band centers. Due to the slightly asymmetric top an asymmetry splitting exists
572 decreasing with increasing K_a . The H_2O dimer exhibits three tunneling motions leading to a sixfold
573 splitting, the largest about 12 cm^{-1} (see [Mukhopadhyay2015] and references therein and [Cole2015]).
574 The splittings change with vibrational state and rotational quantum numbers. The molecule dissociates
575 from the excited vibrational states belonging to the $3\text{ }\mu\text{m}$ bands leading to lifetime broadening which
576 depends on the individual state [Huang1989]. The complex pattern can be seen even at the low
577 temperatures of the rotationally resolved molecular beam spectrum of the librational band in the $20\text{ }\mu\text{m}$
578 region (Figure 2 in [Cole2015]). To find resolved rotational structure at room temperature appears to be
579 unlikely. However, in case of pure rotation some so-called E-type transitions are not much affected by
580 the tunneling splittings and form regular $2B$ -spaced patterns which were observed in ambient
581 temperature water spectra [Tretyakov2013;Serov2014;Koshelev2018] and modelled by [Odintsova2014].
582 Anyhow, the typical shape of a parallel or perpendicular band should approximately be maintained for
583 individual rovibrational bands.

584 In order to model the expected shape of the dimer parallel and perpendicular bands individual
585 rovibrational lines were modelled. Line positions and relative intensities were calculated according to
586 Chapter IV.2 in [Herzberg1945] applying the abovementioned rotational constants ignoring centrifugal
587 distortion and vibrational dependence of rotational constants. In order to account for effects mentioned
588 in the last paragraph causing a rather congested, unresolved spectrum each line was modelled as a 5 cm^{-1}
589 1 HWHM for the parallel and 10 cm^{-1} HWHM Lorentzian for the perpendicular band. This selection was
590 made to smear out individual Q branches in the perpendicular bands and to best approximate the shape
591 of the two narrow features in the observed continuum by the parallel bands. The parallel and
592 perpendicular band shape kernels were assumed to be the same for all rovibrational bands.

593 A more sophisticated method for obtaining rovibrational spectra of the dimer is using *ab initio*
594 calculations involving potential energy and dipole moment surfaces. For the region below 500 cm^{-1} the
595 entire rovibrational spectrum was modelled with this method (see Figure 10 in [Scribano2007]).
596 [Odintsova2019] measured the FIR SC below 50 cm^{-1} and found good agreement with the dimer
597 prediction from [Scribano2007]. Based on the band centers and intensities of the low-lying dimer
598 fundamentals [Kjaergaard2008] we simulated the spectrum using our simplified approach and found
599 coarse agreement regarding overall shape. Certainly, the quality of the *ab initio* calculation depends on
600 the availability of adequate potential energy and dipole moment surfaces. Therefore, the older *ab initio*
601 calculation cited above [Tso1998] with many approximations shows disagreement with the experimental
602 continuum data.

4.2 Fit of self-continuum contributions

As in [Ptashnik2019] the continuum was fitted as the sum of a quasi-bound dimer spectrum and a bound dimer spectrum. The quasi-bound dimer spectrum contribution is modelled from the monomer line positions and intensities given in HITRAN2016 [Gordon2017] (which in turn are taken from [Loos2017]). Ptashnik et al. [Ptashnik2011] estimated from lifetimes that the FWHM should be in the range 14-40 cm^{-1} . The FWHM for the calculation of the quasi-bound dimer from the monomer spectrum in the [Ptashnik2011] and [Ptashnik2019] work was 20 cm^{-1} . We decided to use two cases, FWHM=20 and 40 cm^{-1} . The bound dimer was modelled from band centers and total band intensities where ν_1 and ν_3 were mixed parallel and perpendicular bands and ν_9 purely perpendicular. The kernels described in Section 4.1 were used. The weak ν_2 band was not fitted. It was assumed that the parallel band contribution is 0.5. The integral intensity of the four bands was calculated by averaging the experimental value for Ne matrix in [Ceponkus2008], the experimental value from [Kujanov-Prozument2010], and the theoretical value VPT2 from [Kjaergaard2008]. The mean value was $4.90(41) \times 10^{-17} \text{ cm}^2 \text{ cm}^{-1} / \text{molec}$, where the uncertainty is the maximum difference to the mean. The initial guess for the partitioning of the intensities among the three fundamentals is taken from the averaging and that for the band centers from [Ptashnik2019]. The fractions for ν_3 and ν_1 are used as fit parameters while the fraction for the ν_9 is calculated since the sum of all fractions is 1.

The continuum calculation involves the constants K_{Db} and K_{Dq} . The sum of both constants yields the total dimerization constant K_{eq} . The constants, band centers, intensity partitioning and the fraction of parallel bands, f_{para} , for ν_1 and ν_3 can be fitted. The sum of parallel and perpendicular fractions is 1. The fit results are summarized in Table 2. The statistical uncertainties were too small to be meaningful and thus omitted, considering all the assumptions and approximations. The literature values for the intensity fractions and the band centers are given in the last row. In cases #1 and #2 all parameters were fitted. While in case #1 the FWHM of the Lorentz line shapes was 20 cm^{-1} it was 40 cm^{-1} in case #2. The fitted values agree reasonably with the literature, except for the fraction $f_{\text{S}_{\nu_9}}$ in case #1 and the vibrational band centers of the ν_9 being unphysically high. The dimer fundamentals associated with OH stretching vibrations should be below the monomer values which is in case of the ν_9 dimer band the monomer ν_3 band center at 3756 cm^{-1} [Kjaergaard2008]. Indeed, the value used by [Ptashnik2019], a result of [Kujanov-Prozument2010], is 3749 cm^{-1} which is slightly lower than the monomer value. In case #3 we fixed the band center of the ν_9 to 3749 cm^{-1} . The fitted parallel contribution of ν_1 was above 1 which is unphysical, furthermore, the intensity of the ν_1 is too small and that of ν_9 way too large.

634 Following [Kjaergaard2008] treatment of the vibrations on the basis of donor ν_1 and ν_3 the dipole
635 moment changes with vibration are orthogonal. Assuming that the H-O-H angle of the donor is around
636 104° and the A axis is approximately parallel to the nearly linear O-H-O frame the direction of the dipole
637 moment change has an angle of 52° to the A axis for the donor ν_1 and 38° for the donor ν_3 . This would
638 imply a somewhat greater parallel than perpendicular band contribution for the donor ν_3 . In cases #4
639 and #5 f_{para,ν_1} was fixed to 0.6. The fitted band intensity (see Table 2) of ν_3 agrees reasonably with the
640 literature value (max. difference 13%), and that of ν_1 even better (max. difference 7%). The weakest
641 band (ν_2) among the three considered fundamentals is the worst case, and is 39% stronger than the
642 literature value which is somewhat outside its uncertainty.

643 In cases #6 and #7 the Lorentzian HWHM for the parallel and perpendicular band kernels were doubled.
644 Note that the HWHM for the perpendicular band is a minimum value while for the parallel band it is an
645 approximate optimal value. The doubling should give an estimate of the sensitivity of the fit to these
646 HWHM values. The agreement of the band intensity fractions with literature is worse than for the cases
647 with nominal HWHM. Anyhow, FWHM qD has a larger impact on the dimerization constants than the
648 Lorentzian HWHM of parallel and perpendicular bands.

649

650 Figure 15 shows the observed, calculated, the residuals and the individual contributions to the
651 continuum as well as the calculated bound dimer spectrum for two cases, #1 giving the best residuals,
652 and #4 with larger residuals but physically meaningful parameters. It is remarkable that the residuals in
653 case #1 above 3740 cm^{-1} are very small. The two double maxima of the continuum are clearly linked to
654 the P- and R-branch structure of the respective parallel bands. The constants K_{Db} , K_{Dq} , and K_{eq} were
655 averaged for the cases #4-#7 since they do not contain unphysical results and contain the impacts of
656 changing both the quasi-bound and the bound dimer rovibrational band shapes. Resulting averages are
657 $K_{\text{Db}}=0.026(2)\text{ atm}^{-1}$, $K_{\text{Dq}}=0.044(5)\text{ atm}^{-1}$, and $K_{\text{eq}}=0.070(4)\text{ atm}^{-1}$. The uncertainties given in parentheses
658 reflect only the variation for the selected model changes and are thus a rough estimate. Regarding the
659 well-known $K_{\text{eq}}=0.052\text{ atm}^{-1}$ [Ptashnik2019] the value is too high by 0.018 atm^{-1} . One possible error
660 source is the total band intensity of the bound dimer in the spectral region of interest being too small in
661 the calculations of Kjaergaard [2008]. Indeed, the total band intensity could be too small since some
662 combination bands (with fundamentals $<300\text{ cm}^{-1}$) not accounted for in the calculations may exist in the
663 relevant spectral range. However, an increase of the total band intensity by an unrealistically high value
664 of 50% would decrease K_{eq} only by 0.008 atm^{-1} .

665 An alternative possibility is that 41% of the quasi-bound dimer contribution, corresponding to the 0.018
666 atm^{-1} excess, is caused by middle wing super-Lorentzian effects as suggested by [Serov2017]. This
667 continuum contribution is a factor 6 larger than the foreign-continuum (see Figure 15), as calculated
668 from the areas of SC super-Lorentzian contribution and FC. Let us assume that the in-band FC and the SC
669 contributions have the same physical origin which can be described as super-Lorentzian (see Section
670 5.2). Assuming further that the middle wing super-Lorentzian effect scales the same way as the Lorentz
671 widths when comparing self and foreign Lorentz broadening ($\gamma_{\text{self}} \approx 5 \cdot \gamma_{\text{air}}$), the super-Lorentzian self-
672 continuum contribution should be about 5 times larger than the foreign-continuum. This is indeed
673 comparable to the abovementioned factor 6. Presumably, the middle wing super-Lorentzian contribution
674 has a slightly different shape when compared to the quasi-bound dimer spectrum. In case the shape was
675 similar to the foreign-continuum it could be narrower than the quasi-bound dimer spectrum (see Figure
676 19). We modified the fitting software and mixed 59% of the quasi-bound dimer spectrum with 41% of
677 the FC which was scaled to the area of the quasi-bound dimer spectrum. The fitted results and residuals
678 were similar to the results obtained with the pure quasi-bound dimer spectrum. This shows that in case
679 the middle wing super-Lorentzian contribution of the SC has the same shape as the FC this has only a
680 small influence of the present results. The findings support the proposed presence of middle wing super-
681 Lorentzian monomer contributions. The true dimerization constant, K_{Dq} , for the quasi-bound dimer
682 should then be 0.026 atm^{-1} ($0.044 \text{ atm}^{-1} - 0.018 \text{ atm}^{-1}$).

683 The results should be regarded with care since the band shapes are still a crude approximation
684 neglecting, as mentioned above, hot bands, tunneling splitting, centrifugal distortion, and asymmetry
685 splitting. Furthermore, some weak combination bands are missing. The unphysical solutions of the fit
686 may be linked to such approximations. The larger residuals close to the parallel band centers also show
687 the limitations. In order to calculate approximate experimental dimer spectra the constants K_{Db} and K_{Dq}
688 were fixed to the averages and all other parameters fitted for both FWHM qD cases. The fitted results
689 are listed in cases #8 and #9 in Table 2. A further approximation is to assume the quasi-bound dimer
690 spectra to look exactly as a broadened monomer spectrum. In reality the spectrum of the quasi-bound
691 dimer can be expected to be something in-between bound dimer and monomer spectra, since close to
692 dissociation the distance between the two water molecules increases. Certainly, *ab initio* calculations
693 can cover bound and quasi-bound states, although the transition to two monomers is a challenge.
694 [Scribano2007] did his *ab initio* calculation up to the dissociation limit including several approximations.
695 It is expected that the calculated spectrum already contains some quasi-bound contributions.

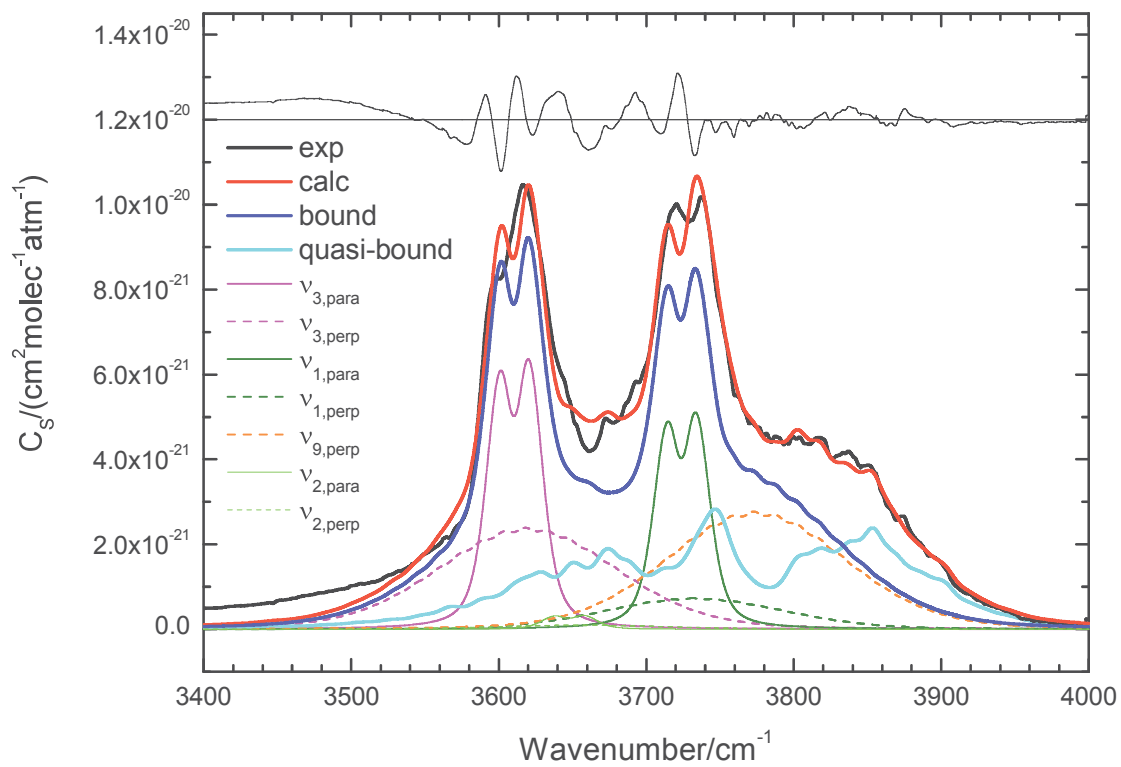
696

697 Table 2. Fit results of SC for cases discussed in the text. Blue bold and black numbers indicate fitted and
698 fixed parameters, respectively. K_{Db} and K_{Dq} are the equilibrium constants for the bound and quasi-bound
699 dimer respectively, with K_{eq} being the sum of these. fS s show the fraction of the total intensity which is
700 assigned to each of the three fundamental bands of the bound dimer, assuming that all the intensity is
701 due to these bands, excluding the weak fundamental. $fpara$ is the fraction of the intensity in each band
702 which is assigned to the contribution to the parallel component (the remainder being due to the
703 perpendicular component - the ν_9 band is assumed to be entirely perpendicular). The fitted band
704 centres for each of these bands is given by ν_o . The assumed full-width half maximum of the quasi-
705 bound dimer contribution is given by FWHM qD . The table has three sections separated by horizontal
706 lines. The first section contains the nominal fits, in the second section the HWHM for the Lorentzian line
707 widths in the parallel and perpendicular dimer bands were doubled, in the lowest section the constants
708 K_{Db} and K_{Dq} were fixed to results obtained in the first section.

#	K_{Db} /atm ⁻¹	K_{Dq} /atm ⁻¹	K_{eq} /atm ⁻¹	fS_{ν_3}	fS_{ν_1}	fS_{ν_9}	$fpara_{\nu_3}$	$fpara_{\nu_1}$	ν_{0,ν_3} /cm ⁻¹	ν_{0,ν_1} /cm ⁻¹	ν_{0,ν_9} /cm ⁻¹	FWHM qD /cm ⁻¹
1	0.029	0.035	0.064	0.48	0.21	0.31	0.44	0.83	3611	3724	3765	20
2	0.027	0.040	0.067	0.48	0.30	0.22	0.47	0.60	3611	3726	3780	40
3	0.031	0.039	0.070	0.44	0.12	0.44	0.44	1.25	3611	3723	3749	20
4	0.025	0.042	0.067	0.48	0.27	0.25	0.54	0.6	3610	3724	3749	20
5	0.024	0.050	0.074	0.49	0.30	0.21	0.55	0.6	3610	3726	3749	40
6	0.028	0.038	0.066	0.42	0.32	0.26	0.76	0.6	3611	3724	3749	20
7	0.026	0.047	0.073	0.43	0.36	0.21	0.78	0.6	3611	3725	3749	40
8	0.026	0.044	0.070	0.47	0.35	0.18	0.52	0.51	3610	3724	3776	20
9	0.026	0.044	0.070	0.49	0.31	0.20	0.49	0.61	3611	3726	3776	40
lit				0.55(8)	0.28(6)	0.18(3)			3597	3730	3749	

709

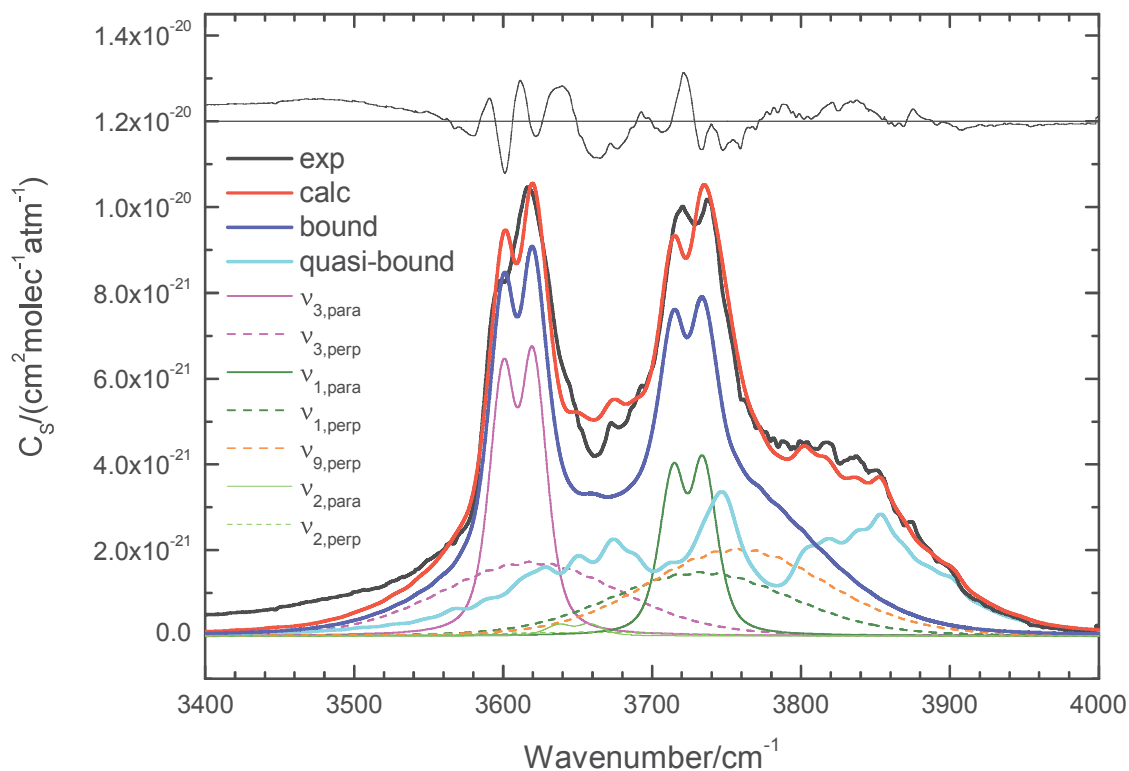
710



711

712

713



714
 715 Figure 15. Observed and fitted SC at 296 K. Top: case #1 in Table 2, bottom: case #4 in Table 2. Thick
 716 black: Observed SC, thick red: calculated SC, thick blue: sum of bound dimer contributions, thick cyan:
 717 quasi-bound dimer contribution, magenta, green, orange, light green: ν_3 , ν_1 , ν_9 , ν_2 bound dimer
 718 contributions. The four broad features are perpendicular bound dimer bands (dashed) while the
 719 narrower double-peak features are parallel bound dimer bands (solid). Note: The ν_9 has only a
 720 perpendicular contribution. Residuals of the fit offset by $1.2 \times 10^{-20} \text{ cm}^2 \text{ molec}^{-1} \text{ atm}^{-1}$ are shown in black.

721 5. Discussion

722 5.1 Self-continuum

723 Comparison with other work

724 The SC for 296 K and 353 K is compared to the CAVIAR work for 293 K and 351 K ([Paynter2009],
 725 downloaded from <http://www.met.reading.ac.uk/caviar/home/data.php>) and to MT_CKD3.2 in Figure
 726 17. There are further experimental data cited in Section 1.4. Comparison of these earlier data with the

727 CAVIAR work can be found in Figure 6 in [Paynter2009] and in Figure 2 in [Ptashnik2019]. The CAVIAR
728 293 K SC is in good agreement with the present data between 3600 and 3800 cm^{-1} . However, inspection
729 of the uncertainties and the differences between the present work and [Paynter2009], shown in Figure
730 18, exhibits significant discrepancies at both higher and lower wavenumbers. The uncertainties of the
731 present work are up to a factor 20 smaller above 3550 cm^{-1} , especially in the intense region of the
732 monomer band. However, below 3550 cm^{-1} the stated CAVIAR uncertainties are smaller by a factor 5.
733 The CAVIAR work shows large gaps and spectral structures which are not present in the new work. The
734 SC differences are largest in the region where the monomer has strong lines and are in the range 0-10%
735 of the strongest continuum features. The differences are outside the uncertainties stated for the CAVIAR
736 work below 3550 cm^{-1} by up to a factor 10. The differences in this region appear to be a systematic error
737 in the CAVIAR data since in Figure 7 the SC derived from independent air-broadened measurements
738 agrees much better with the present results. Above 3550 cm^{-1} most data points are within the CAVIAR
739 uncertainties. Regarding the uncertainties of the present work the differences are up to 10 times larger.
740 In conclusion the present method for continuum determination yields substantial improvements. The
741 differences between the present and the CAVIAR work reflect the impact of the different methods. The
742 present method uses the entire spectrum, has thus no gaps and hence more information, but is very
743 sensitive to the accurate representation of local lines. The CAVIAR method uses microwindows with
744 smaller dependence on local lines. Furthermore, in case of the CAVIAR method the local line parameters
745 are taken from spectroscopic databases and not from the spectra used to derive the continuum. Thus,
746 errors from local lines do still exist although the sensitivity to local line errors is probably smaller than for
747 the new method. Figure 17 shows that agreement of the high temperature data with CAVIAR is also
748 reasonable. However, as already stated before, due to lack of sufficient measurements, the data quality
749 of the present work's high temperature data is bad and the CAVIAR data are expected to be of much
750 better quality.

751 Figure 17 also shows that the MT_CKD3.2 continuum model (and its earlier versions – see [Paynter2009])
752 is significantly weaker (by almost a factor of 10 at 3600 cm^{-1}) than the observed spectra between around
753 3500 and 3750 cm^{-1} and misses the two marked peaks near 3620 and 3730 cm^{-1} . We interpret that as
754 being due to the fact that the MT_CKD3.2 continuum model does not include the bound dimer spectrum.

755 From the temperature dependence on Figure 17 it can clearly be seen that the continuum consists of
756 two parts. One part (at wavenumbers below about 3800 cm^{-1}) looks similar to the modelled dimer
757 spectrum and has a stronger temperature dependence. In Figure 5D in [Ptashnik2011] it can be seen that
758 the ratio of SC(293 K) and SC(351 K) is about 2.7 at the pronounced dimer bands and about 2.0 away

759 from the bands. The temperature dependence of the in-band SC is investigated in detail in
760 [Ptashnik2019].

761

762 **Dimer band shape and dimerization constants**

763 In the present work the dimer rovibrational band shape was modelled taking into account the expected
764 band structure and type based on results of high resolution spectroscopy mostly in molecular beams.
765 This allowed fitting of the SC resulting in tentative experimental dimer spectra which differ significantly
766 from the prediction used in [Ptashnik2019]. In their work they fitted continua at different temperatures
767 to a sum of modelled dimer bands and a quasi-bound dimer contribution calculated with a Voigt FWHM
768 of 20 cm⁻¹. Residuals were up to 20% between 3550 and 3650 cm⁻¹ and 45% around 3780 cm⁻¹, the
769 modelled values are systematically too high above 3850 cm⁻¹ (see Figure 5, ν_3 , 296 K in [Ptashnik2019]).
770 The fitted constants were $K_{Db}=0.020(6)$ atm⁻¹ and $K_{Dq}=0.071(26)$ atm⁻¹. In the present work the
771 corresponding values are 0.026(2) atm⁻¹ and 0.044(5) atm⁻¹. While the K_{Db} values are similar the K_{Dq} value
772 is smaller by 0.03 atm⁻¹. The residuals in the present work are of similar size around 3600 cm⁻¹ but the
773 agreement of the structure of the two peaks is better. Furthermore, the residuals around 3780 cm⁻¹ are
774 significantly smaller and the residuals above 3850 cm⁻¹ are smaller, too.

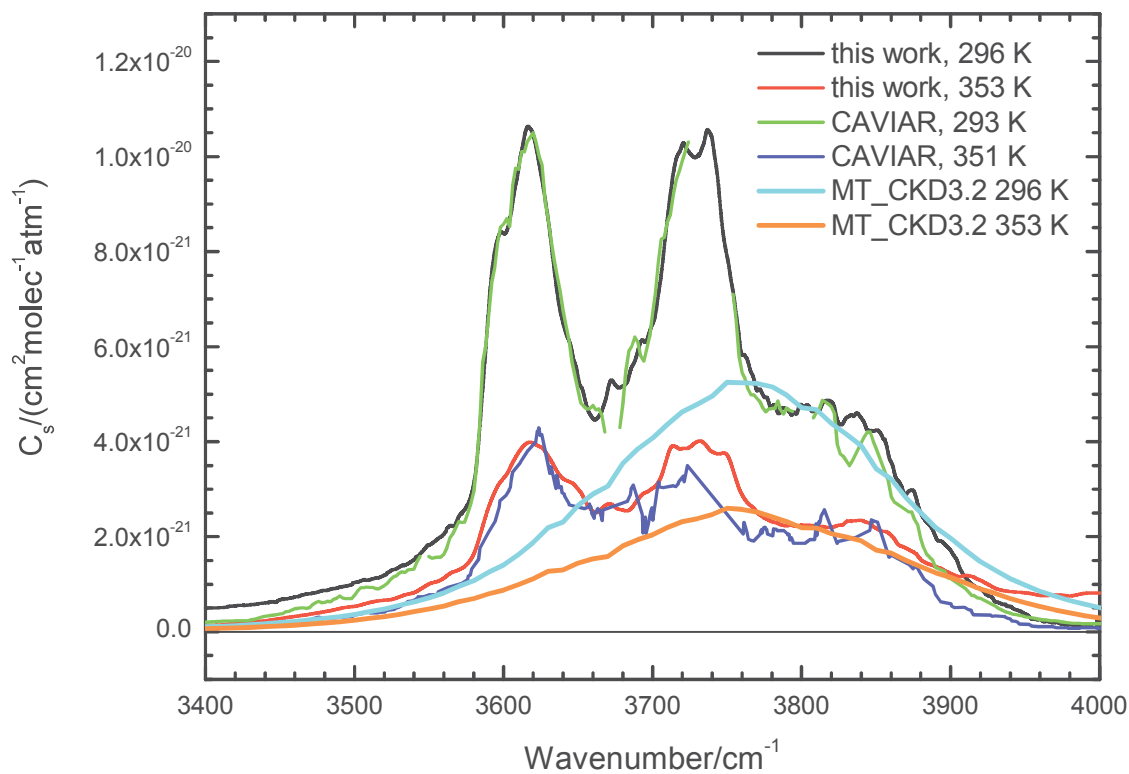
775 **Non-Lorentzian line wings as third SC component**

776 As stated above [Serov2017] postulates that line wings of the monomer band that differ from the Voigt
777 profile are a third component of the SC needed to resolve the discrepancy of the too large observed
778 quasi-bound dimer spectrum when compared to the prediction from the equilibrium constant for the
779 quasi-bound dimer. A multiplicative correction function for the Voigt profile, similar to the MT_CKD
780 approach (see above), was defined. The parameter Δv_{wing} was fixed to 11 cm⁻¹ which leads to
781 pronounced structures in the continuum (see Figure 2b in [Serov2017]). This had been based on the
782 structures observed in the CAVIAR data which may result from limitations in the measurements or
783 analysis since the SC in the present work looks significantly smoother (Figure 17) and has been validated
784 by quality checks (see e.g. Figure 9). The structures observed in the CAVIAR data may be linked to the
785 structure of the monomer spectrum itself, through the analysis process which uses troughs in the
786 spectrum in combination with possibly erroneous local line parameters. Serov even uses the “spectral
787 heterogeneity” to prove the non-Voigt line wing contribution to the continuum: that paper states that
788 “The monomolecular nature of the excess continuum is also indirectly confirmed by its spectral
789 heterogeneity. The dimeric absorption (a tremendous number of collisionally-broadened lines, which are
790 more or less uniformly spread over the range) is very smooth. The spectrum of free-pairs is even

791 smoother due to the very short collision time causing the absorption. Therefore, the heterogeneity of
792 the spectrum is the evidence that it belongs to the monomer line wings. A similar non-monotonicity of
793 the water continuum, which is comparable with its measurement error in each separate transparency
794 window, can be found in all wideband studies". The present work certainly does not support these
795 statements. This does not rule out the line wing contribution but Δv_{wing} must be substantially larger.
796 However, the argument that the continuum structure proves the existence of a structured line wing
797 contribution is not valid. Recently, [Odintsova2019] reported about the far-infrared pure rotation SC and
798 found strong structure between 100 and 300 cm^{-1} which was tentatively attributed to local line problems
799 and not to a structured SC.

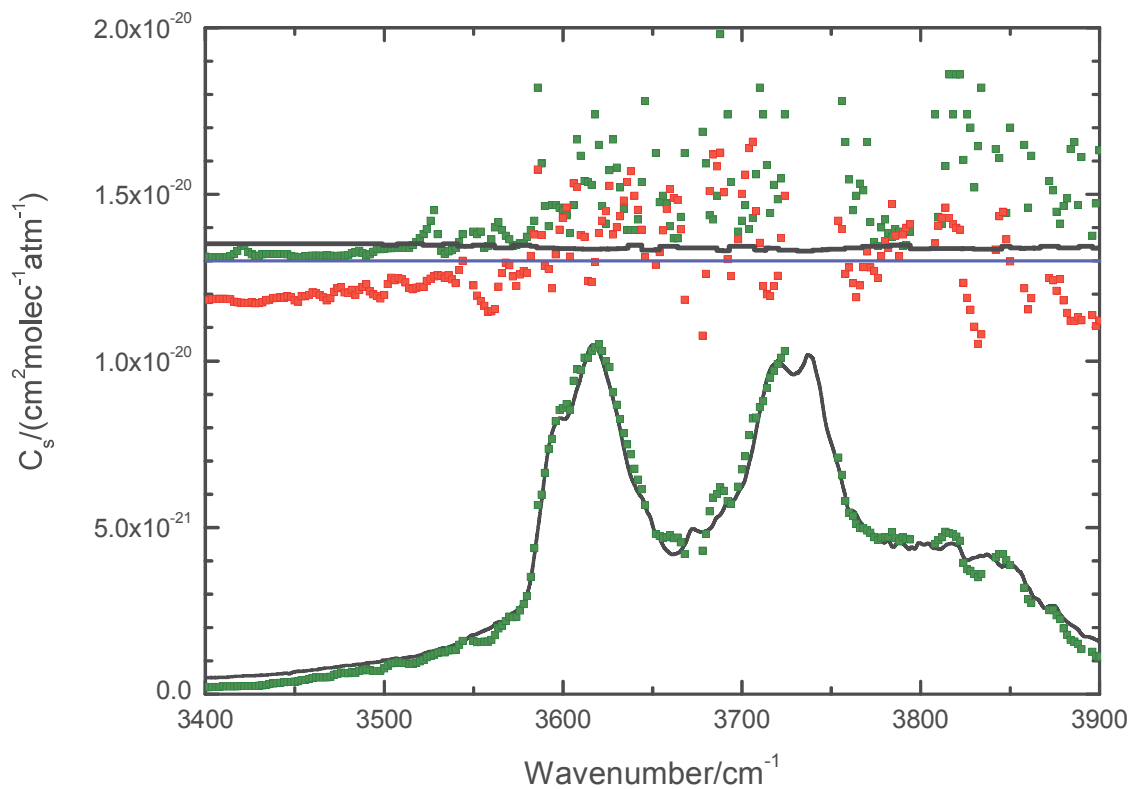
800 As shown above, the results of the present work indicate the presence of a middle wing super-Lorentzian
801 contribution. However, there was no high resolution structure found in contrast to Serov's results. The
802 magnitude of the middle wing super-Lorentzian contribution suggests similarities with the FC which also
803 does not show high resolution structure.

804



805

806 Figure 17. Comparison between different SCs and the dimer spectrum around 296 K. Experimental data
807 at ca. 350 K are also shown. The base term [Paynter2009] was added to the SC from the current work in
808 order to make it comparable to the other work. The wing correction applied for the FC (see below) could
809 be neglected. CAVIAR data have been downloaded from
810 <http://www.met.reading.ac.uk/caviar/home/data.php>.



811
812 Figure 18. Comparison of CAVIAR and this work. Lower traces: black: SC this work, green: SC CAVIAR,
813 upper traces multiplied by 4 and offset by $1.3 \times 10^{-20} \text{ cm}^2 \text{ molec}^{-1} \text{ atm}^{-1}$: black: uncertainty this work, green:
814 uncertainty CAVIAR, red: CAVIAR - this work. CAVIAR data have been downloaded from
815 <http://www.met.reading.ac.uk/caviar/home/data.php>.

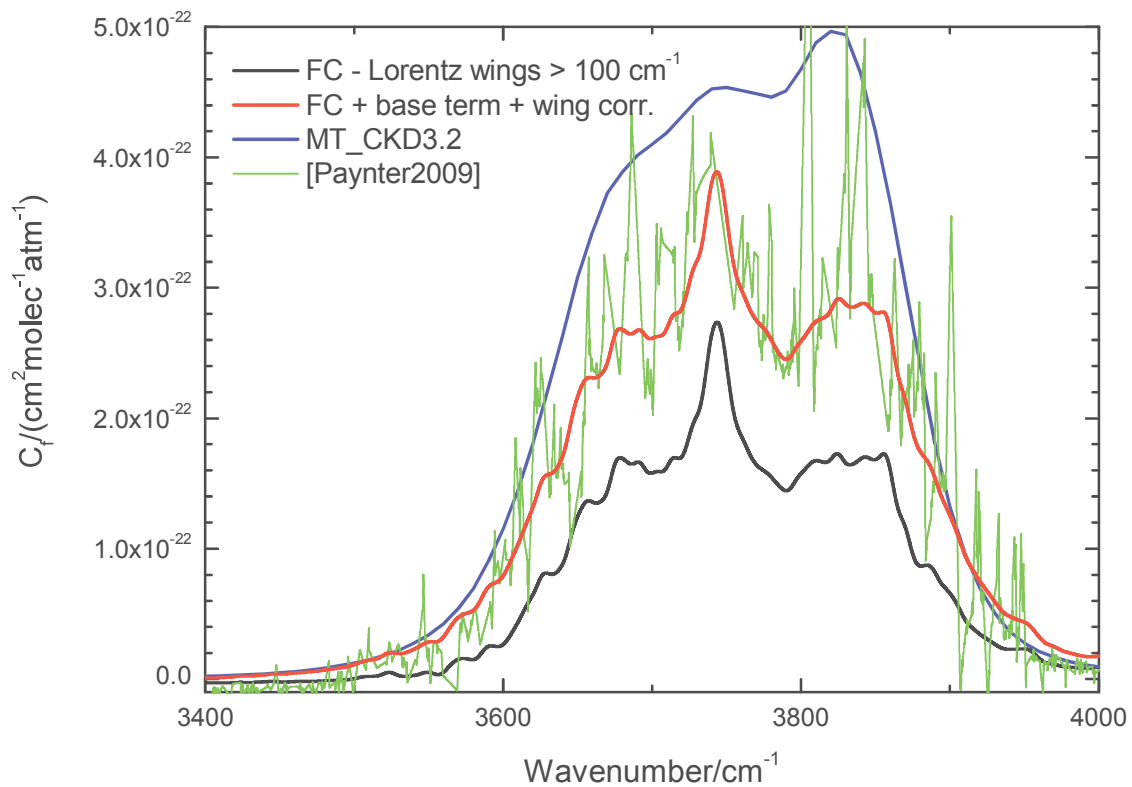
816

817 5.2 Foreign-continuum

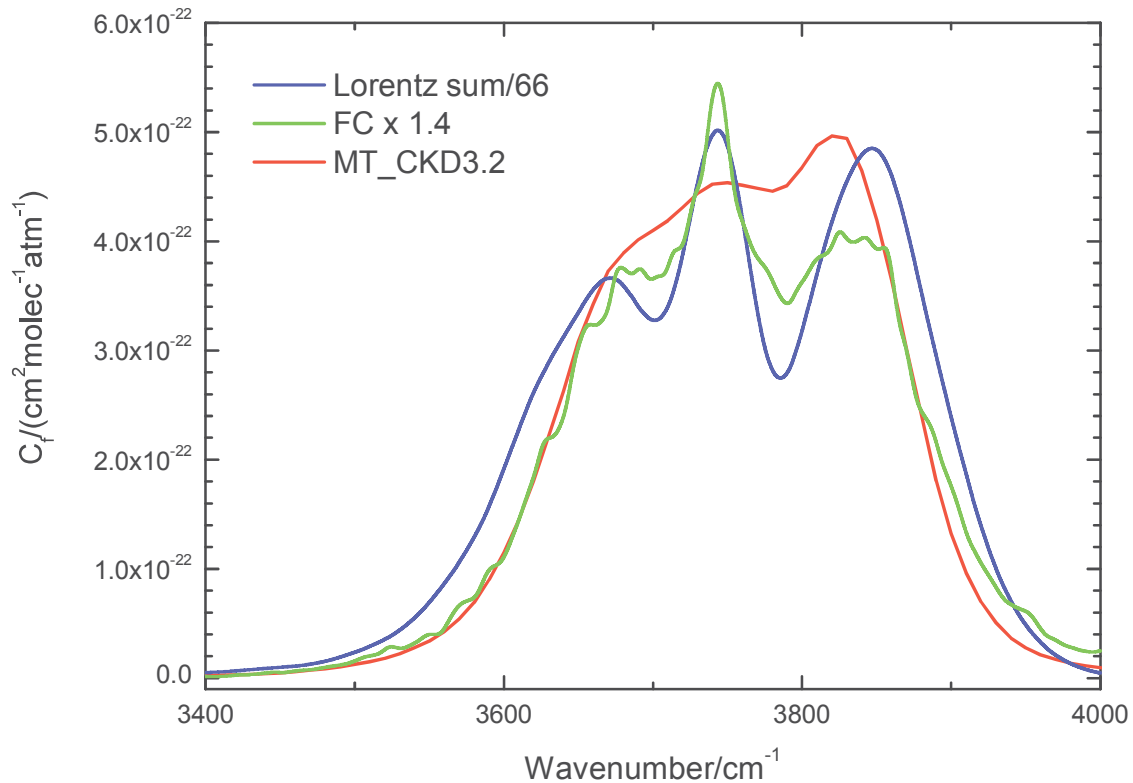
818 The FC for 296 K is compared to MT_CKD3.2 and the [Paynter2009] work in Figure 19. The base term had
819 to be added to the FC of this work for intercomparison. It should be noted that the base term was
820 introduced in the MT_CKD continuum model to ensure a smooth continuum [Mlawer2012]. For each line
821 the intensity of the Lorentzian profile at 25 cm^{-1} away from the line center is taken to be part of the
822 continuum for the whole spectral range $\pm 25\text{ cm}^{-1}$ from the line center. The base term is the sum of all
823 these “plinths”. Furthermore, the sum of all line contributions $>25\text{ cm}^{-1}$ and $>100\text{ cm}^{-1}$ from line centers
824 were calculated. Recall that the multispectrum fit cuts line profiles 100 cm^{-1} from line centers. In order to
825 compare the original FC to Paynter and MT_CKD the $>25\text{ cm}^{-1}$ contribution has to be added and the >100
826 cm^{-1} contribution has to be subtracted. This is equivalent to adding the missing contributions $25\text{-}100\text{ cm}^{-1}$.
827 The Paynter continuum is very noisy but on average shows good agreement with the present work.
828 The MT_CKD3.2 FC is on average ca. 40% larger and has a significantly different shape, not showing P, Q
829 and R-branch structure in contrast to the FC from the present work and the monomer band (see Figure
830 20). The black curve on Figure 19 is the FC without any local Voigt lines contribution.. We call this
831 “physical continuum” because it contains only contributions not covered by the untruncated line model.
832 In Figure 20 the smoothed monomer band, the MT_CKD3.2 continuum model and the red curve from
833 Figure 19 are shown. While the MT_CKD3.2 continuum model and the FC from the present work have
834 the same width, it is notable that they are narrower than the monomer band. The physical continuum
835 from Figure 19 is even narrower. It was assured that the selection of the smoothing parameter has no
836 significant influence on the apparent width of the monomer band. The mathematics causing the
837 MT_CKD continuum model to be narrower than the monomer band can be found in [Mlawer2012] who
838 introduced a lower state energy dependent weighting (see Eq. 3.3 therein) which decreases the weight
839 in the wings of P- and R-branch, where transitions with high lower state energy dominate.

840 Concerning the physical nature of the FC there may be a link to the paper of [Tran2017] where HCl Argon
841 broadening was measured and theoretically investigated. rCMDS (requantized Classical Molecular
842 Dynamics Simulations) calculations were carried out in order to theoretically predict the line shape.
843 rCMDS is based on purely classical trajectory calculations followed by re-establishing the quantized
844 states. For details the reader is referred to [Tran2017] and references therein. The ratios of absorption
845 cross sections in the troughs and the Lorentz values (fitted from the measurement) are similar to the
846 ratios of calculated rCMDS absorption cross sections to Lorentz values fitted to rCMDS absorption cross
847 sections. It should be mentioned that the Lorentzian widths deduced from the measurement and those
848 obtained from rCMDS calculations show significant differences (see Figure 3 in [Tran2017]). So rCMDS
849 appears to be good to calculate deviations from ideal behavior but not the lineshape in an absolute

850 manner. The dipole auto-correlation function was fitted to an expression which in the spectral domain
 851 was approximated by the sum of three Lorentzians. This sum can explain the super-Lorentzian behavior
 852 close to band center but not the sub-Lorentzian behavior for the band wings: [Tran2017] state that “the
 853 observed non-Lorentzian absorption results from two competitive mechanisms: (i) the behavior of the
 854 dipole autocorrelation at short times (related with collisions that are ongoing or start at $t = 0$) which
 855 induces super-Lorentzian effects; (ii) line-mixing (i.e., transfers of populations among the rotational
 856 levels) that reduces the absorption in the band wings and high J line regions and induces sub-Lorentzian
 857 effects.” It is interesting to see that the FC has some similarity to the HCl/Ar spectra where intensity is
 858 transferred from the band wings to the band center. That the FC is narrower than the monomer band
 859 could also indicate an intensity transfer from the band wings to the center. Furthermore, a sub-
 860 Lorentzian behavior in the in-between band region also exists for the H₂O FC (see [Wagner2020]).



861
 862 Figure 19. Comparison of FC. Wing correction refers to adding line contributions >25 cm^{-1} from line
 863 center and subtracting those >100 cm^{-1} . FC is obtained from the baseline fits of the present work. The
 864 black curve is the FC without any local lines Voigt contribution.



866

867 Figure 20. Comparison of MT_CKD3.2 FC with scaled smoothed Lorentz sum (smoothing kernel FWHM =
 868 5 cm^{-1} , Lorentz HWHM = 0.5 cm^{-1} , parameters selected to show the low-resolution band shape) and
 869 scaled FC from present work. Scaling was introduced to have similar amplitude for better comparison.

870

871 6. Conclusion

872 A new method to derive the in-band SC and FC was developed. The method uses the same spectra to
 873 derive local line parameters and continua. It is essential to fit the local lines down to approximately the
 874 noise level to ensure that the fitted baseline only contains continuum information. The Hartmann-Tran
 875 profile in combination with Rosenkranz line mixing was required for accurate local line fitting. The
 876 method allowed the determination of the in-band SC for H_2O at 296 K in the $3 \mu\text{m}$ region without gaps
 877 and high spectral resolution of 2.4 cm^{-1} . Even in microwindows which were almost opaque, baseline and

878 thus continuum information was still available. In the case of the FC at 296 K there are also no gaps and
879 the resolution was 7-16 cm^{-1} . The uncertainty in the FC was larger due to the high pressures and thus
880 more congested spectra. Furthermore, the SC is also visible in the air-broadened spectra and thus SC
881 errors are propagated into the FC. The new method for determining the continuum has led to
882 considerably improved information content for SC and FC. Quality checks were used to validate the fitted
883 continua. First, the SC was fitted from air-broadened measurements only and found to be in excellent
884 agreement when compared with the SC from the self-broadened measurements. Second, residuals
885 calculated from the original spectra and spectra modelled using local line parameters together with the
886 continua are almost noise. SC and FC were also determined for 353 K, both from air-broadened
887 measurements, but with less quality than the 296 K results due to the limited set of measurements.

888 Although the new self-continuum agrees well with the CAVIAR results between 3600 and 3800 cm^{-1} there
889 are differences which exceed the uncertainties at higher and lower wavenumber. A significant advantage
890 of the new self-continuum is that it is much smoother, has no gaps and is obtained with a high resolution
891 of 2.4 cm^{-1} . The differences between the present and the CAVIAR work reflect the impact of the
892 different methods. The new method uses the entire spectrum, has thus no gaps hence more
893 information, but is very sensitive to the accurate representation of local lines. The CAVIAR method used
894 microwindows with small dependence on local lines. Furthermore, the local line parameters are taken
895 from spectroscopic databases and not from the spectra used to derive the continuum. Thus, errors from
896 local lines do still exist although the sensitivity to local line errors is probably smaller than for the new
897 method. The MT_CKD3.2 SC shows no bound dimer bands and differs significantly from both
898 experimental SC datasets.

899 The self-continuum was fitted as sum of modeled bound and quasi-bound dimer spectra. From rotational
900 constants the bound dimer parallel and perpendicular band shapes of the near prolate symmetric top
901 molecule were calculated. Among the three strong dimer fundamentals in the 3 μm region, those linked
902 to the H-O stretching vibration of the donor molecule, ν_1 and ν_3 , have both parallel and perpendicular
903 components while the asymmetric H-O stretch of the acceptor molecule, ν_9 , is of purely perpendicular
904 type. The quasi-bound dimer band shape was calculated from the spectroscopic database of the H_2O
905 monomer for two cases with Voigt FWHM 20 cm^{-1} and 40 cm^{-1} for all lines. For the bound dimer
906 fundamental wavenumbers, relative band intensities and partitioning of parallel and perpendicular band
907 type were fitted, while the integral of the band intensities of the four fundamentals was fixed to
908 published experimental/theoretical data. Dimerization constants for bound and quasi-bound dimers

909 were also fitted. The new approach allows modelling the observed continuum with unprecedented
910 quality. Fit results for the H₂O dimer band centers and intensities were in reasonable agreement with
911 experimental/theoretical literature data. In order to obtain physically meaningful results the band center
912 of ν_9 as well as the parallel band contribution of ν_1 had to be fixed. A dimerization constant for the
913 bound dimer of $K_{Db}=0.026(2)$ atm⁻¹ and the quasi-bound dimer of $K_{Dq}=0.044(5)$ atm⁻¹ was fitted. The sum,
914 the total dimerization constant, was found to be too large by 0.018 atm⁻¹ when compared to literature
915 values. The excess was tentatively attributed to middle line wing super-Lorentzian contributions of the
916 H₂O monomer lines, resulting in a dimerization constant for the quasi-bound dimer of $K_{Dq}'=0.026$ atm⁻¹.

917 We suggest applying the fit procedure introduced in the present work also to the continuum data at
918 temperatures other than 296 K, published in [Ptashnik2019]. The temperature dependence may provide
919 more insights on the nature of contributions to the in-band SC. The investigation of other strong
920 fundamental regions, like the bands around 1600 cm⁻¹, applying the new method would furthermore
921 improve the understanding on the continuum.

922 The FC at 296 K agrees with the Paynter results but is much less noisy and has no gaps in spectral
923 coverage. It is on average about 40% smaller than the MT_CKD3.2 FC model and shows a very different
924 shape. It has a pronounced P, Q, and R branch structure barely visible in the more noisy Paynter results.
925 Both, the FC from present work and the MT_CKD FC model appear narrower than the monomer band
926 which may be of interest regarding the physical nature of the FC. Certainly, the new method has larger
927 benefits for FC than SC determination since the impact of local lines is larger for the FC due to the higher
928 pressure needed (resulting in broader lines) since the FC is much weaker than the SC.

929 The method presented here will be improved by fitting the continuum and line parameters
930 simultaneously in the multispectrum fitting approach. Certainly, dedicated measurements with
931 optimized pressure and temperature steps and high baseline quality will help to provide excellent
932 continuum data with the new method, which can be extended to derive the continuum in other water
933 vapor bands.

934

935 **Acknowledgements**

936 The measurement of the spectra and the previous line parameter analysis have been performed within
937 the framework of the DFG projects under contract numbers BI 834/5-1 and BI 834/5-2. KPS

938 acknowledges support from the UK Natural Environment Research Council (grant number
939 NE/R009848/1). The authors thank David Paynter for providing the data in Figure 19 in digital form and
940 for answering queries, and the reviewers of the original submission this paper for triggering several
941 essential improvements.

942

943 **Appendix A. Supplementary material**

944 Supplementary data associated with this article can be found in the online version at
945 <http://dx.doi.org/....> FC and SC at 296 K together with uncertainties are given in ASCII files
946 FC_H2O_3mu.txt and SC_H2O_3mu.txt, first column wavenumber, second column continuum coefficient
947 in $\text{cm}^2\text{molec}^{-1}\text{atm}^{-1}$, third column uncertainty in $\text{cm}^2\text{molec}^{-1}\text{atm}^{-1}$.

948

949 **References**

950

951 [Birk2016] Birk M, Wagner G. Voigt profile introduces optical depth dependent systematic errors -
952 Detected in high resolution laboratory spectra of water. J Quant Spectrosc Radiat Transfer 2016;170:159-
953 168. <http://doi.org/10.1016/j.jqsrt.2015.11.008>.

954 [Burch1982] Burch DE. Continuum absorption by H₂O. AFGL-TR 1982;81:0300.
955 <http://dx.doi.org/10.1117/12.931899>.

956 [Burch1984] Burch DE, Alt RL. Continuum absorption by H₂O in the 700-1200 cm⁻¹ and 2400-2800 cm⁻¹
957 windows. AFGL-TR 1982;84:0128.

958 [Burch1985] Burch, DE, Absorption by H₂O in narrow windows between 3000 - 4200 cm⁻¹, AFGL-TR
959 1985;85-0036. Air Force Geophys. Lab., Hanscom AFB, Mass.

960 [Campargue2016] Campargue A, Kassi S, Mondelain D, Vasilchenko S, Romanini D. Accurate laboratory
961 determination of the near-infrared water vapor selfcontinuum: A test of the MT_CKD model. J Geophys
962 Res Atmos 2016;121:13,180-13,203. <http://doi.org/10.1002/2016JD025531>.

963 [Ceponkus2008] Ceponkus J, Uvdal P, Nelander B. Far-Infrared Band Strengths in the Water Dimer:
964 Experiments and Calculations. J. Phys. Chem. A 2008;112:3921-3926. <http://doi.org/10.1021/jp711178w>.

965 [Clough1989] Clough SA, Kneizys FX, Davies RW. Line Shape and the Water Vapour Continuum. Atm Res
966 1989;23:229-41. [http://dx.doi.org/10.1016/0169-8095\(89\)90020-3](http://dx.doi.org/10.1016/0169-8095(89)90020-3).

967 [Cole2015] Cole WTS, Fellers RS, Viant MR, Leforestier C, Saykally RJ. Far-infrared VRT spectroscopy of
968 the water dimer: Characterization of the 20 μm outof-plane librational vibration. J. Chem. Phys
969 2015;143:154306. <http://dx.doi.org/10.1063/1.4933116>.

970 [Cormier2005] Cormier JG, Hodges JT, Drummond JR. Infrared water vapour continuum absorption at
971 atmospheric temperatures, J Chem Phys 2005;122:114309. <http://doi.org/10.1063/1.1862623>.

972 [Epifanov1997] Epifanov SYu, Vigasin AA. Subdivision of phase space for anisotropically interacting water
973 molecules. Mol. Phys. 1997;90(1):101-106.

974 [Gordon2017] Gordon IE, Rothman LS, Hill Chr, Kochanov R, Yan T, Bernath PF, Birk M, Boudon V,
975 Camparque A, Chance K, Drouin BJ, Flaud J-M, Gamache RR, Hodges JT, Jacquemart D, Perevalov VI,
976 Perrin A, Shine KP, Smith MAH, Tennyson J, Toon GC, Tran H, Tyuterev VIG, Barbe A, Csaszar A, Devi V,
977 Loos J, Wagner G, Wilzewski J, et al. The HITRAN2016 Molecular Spectroscopic Database, J Quant
978 Spectrosc Radiat Transfer 2017;203:3-69. <http://doi.org/10.1016/j.jqsrt.2017.06.038>.

979 [Herzberg1945] Herzberg G. Molecular spectra nad molecular structure, II. Infrared and Raman spectra
980 of polyatomic molecules. Van Nostrand, New York.

981 [Huang1988] Huang ZS, Miller RE. Sub-Doppler resolution infrared spectroscopy of water dimer. J. Chem.
982 Phys. 1988;88:8008. <http://doi.org/10.1063/1.454258>.

983 [Huang1989] Huang ZS, Miller RE. High-resolution near-infrared spectroscopy of water dimer. J. Chem.
984 Phys. 1989;91:6613. <http://doi.org/10.1063/1.457380>.

985 [Kapitanov2018] Kapitanov VA, Osipov KY, Ptashnik IV. Photoacoustic measurements of the water vapor
986 continuum absorption in the 1.6 μm window, Optika Atmosfery i Okeana 2018;31:995-1000, in Russian

987 [Kjaergaard2008] Kjaergaard HG, Garden AL, Chaban GM, Gerber RB, Matthews DA, Stanton JF.
988 Calculation of Vibrational Transition Frequencies and Intensities in Water Dimer: Comparison of Different
989 Vibrational Approaches. J Phys Chem A 2008;112:4324-4335. <http://doi.org/10.1021/jp710066f>.

990 [Koshelev2018] Koshelev MA, Leonov II, Serov EA, Chernova AI, Balashov AA, Bubnov GM, Aleksandr FA,
991 Shkaev AP, Parshin VV, Krupnov AF, Tretyakov MYu. New Frontiers in Modern Resonator Spectroscopy.
992 IEEE TRANSACTIONS ON TERAHERTZ SCIENCE AND TECHNOLOGY 2018;8:773-783.
993 <http://doi.org/10.1109/TTHZ.2018.2875450>.

994 [Kuyanov-Prozument2010] Kuyanov-Prozument K, Choi MY, Vilesov AF. Spectrum and infrared intensities
995 of OH-stretching bands of water dimers. J Chem Phys 2010;132:014304.
996 <http://doi.org/10.1063/1.3276459>.

997 [Kuyanov-Prozument2010] Kuyanov-Prozument K, Choi MY, Vilesov AF. Spectrum and infrared intensities
998 of OHstretching bands of water dimers. J Chem Phys 2010;132:014304.

999 [Lechevallier2018] Lechevallier L, Vasilchenko S, Grilli R, Mondelain D, Romanini D, Campargue A. The
1000 water vapour self-continuum absorption in the infrared atmospheric windows: new laser measurements
1001 near 3.3 and 2.0 μm . Atmos Meas Tech 2018;11:2159–2171. <http://doi.org/10.5194/amt-11-2159-2018>.

1002 [Loos2017] Loos J, Birk M, Wagner G. Measurement of positions, intensities and self-broadening line
1003 shape parameters of H₂O lines in the spectral ranges 1850-2280 cm⁻¹ and 2390-4000 cm⁻¹. J Quant
1004 Spectrosc Radiat Transfer 2017;203:119-32. <http://doi.org/10.1016/j.jqsrt.2017.02.013>.

1005 [Loos2017a] Loos J, Birk M, Wagner G. Measurement of air-broadening line shape parameters and
1006 temperature dependence parameters of H₂O lines in the spectral ranges 1850-2280 cm⁻¹ and 2390-4000
1007 cm⁻¹. J Quant Spectrosc Radiat Transfer 2017;203:103-18. <http://doi.org/10.1016/j.jqsrt.2017.03.033>.

1008 [Ma2008] Ma Q, Tipping RH, Leforestier C, Temperature dependences of mechanisms responsible for the
1009 water-vapour continuum absorption. I. Far wings of allowed lines, J Chem Phys 2008;128:124313.
1010 <http://doi.org/10.1063/1.2839604>.

1011 [Mlawer2012] Mlawer EJ, Payne VH, Moncet J-L, Delamere JS, Alvarado MJ, Tobin DC. Development and
1012 recent evaluation of the MT_CKD model of continuum absorption. Phil Trans R Soc A 2012;370:2520-56.
1013 <http://dx.doi.org/10.1098/rsta.2011.0295>.

1014 [Mlawer2019] Mlawer EJ, Turner DD, Paine SN, Palchetti L, Bianchini G, Payne VH, et al. Analysis of water
1015 vapor absorption in the far-infrared and submillimeter regions using surface radiometric measurements
1016 from extremely dry locations. J Geophys Res: Atmospheres 2019;124:8134-8160.
1017 <https://doi.org/10.1029/2018JD029508>.

1018 [Mondelain2015] Mondelain D, Vasilchenko S, Cermak P, Kassi S, Campargue A. The self- and foreign-
1019 absorption continua of water vapor by cavity ring-down spectroscopy near 2.35 μm. Phys Chem Chem
1020 Phys 2015;17:17762. <http://doi.org/10.1039/C5CP01238D>.

1021 [Mondelain2020] Mondelain D, Vasilchenko S, Kassi S, Campargue A. The water vapor foreign-continuum
1022 in the 1.6 μm window by CRDS at room temperature. J Quant Spectrosc Radiat Transfer
1023 2020;246:106923. <https://doi.org/10.1016/j.jqsrt.2020.106923>.

1024 [Mukhopadhyay2015] Mukhopadhyay A, Cole WTS, Saykally RJ. The water dimer I: Experimental
1025 characterization. Chem Phys Let 2015;633:13-26. <http://doi.org/10.1016/j.cplett.2015.04.016>.

1026 [Newman2012] Newman et al., Airborne and satellite remote sensing of the mid-infrared water vapour
1027 continuum, Phil Trans R Soc A 2012;370:2611-2636. <http://dx.doi.org/10.1098/rsta.2011.0223>.

1028 [Odintsova2014] Odintsova TA, Tretyakov MYu, Krupnov AF, Leforestier C. The water dimer millimeter-
1029 wave spectrum at ambient conditions: A simple model for practical applications. J Quant Spectrosc
1030 Radiat Transfer 2014;140:75–80. <http://dx.doi.org/10.1016/j.jqsrt.2014.02.016>

1031 [Odintsova2019] Odintsova TA, Tretyakov MYu, Zibarova AO, Piralı O, Roy P, Campargue A. Far-infrared
1032 self-continuum absorption of H₂¹⁶O and H₂¹⁸O (15–500 cm⁻¹). J Quant Spectrosc Radiat Transfer
1033 2019;227:190–200. <http://dx.doi.org/10.1016/j.jqsrt.2019.02.012>.

1034 [Paynter2009] Paynter DJ, Ptashnik IV, Shine KP, Smith KM, McPheat R, and Williams RG. Laboratory
1035 measurements of the water vapour continuum in the 1200–8000 cm⁻¹ region between 293 K and 351 K, J
1036 Geophys Res 2009;114:D21301. <http://dx.doi.org/10.1029/2008JD011355>.

1037 [Paynter2011] Paynter DJ, Ramaswamy V. An assessment of recent water vapor continuum
1038 measurements upon longwave and shortwave radiative transfer. J Geophys Res 2019;116:D20302.
1039 <http://dx.doi.org/10.1029/2010JD015505>.

1040 [Ptashnik2004] Ptashnik IV, Smith KM, Shine KP, Newnham DA. Laboratory measurements of water
1041 vapour continuum absorption in spectral region 5000–5600 cm⁻¹: Evidence for water dimers
1042 Quart J Roy Met Soc 2004;130:2391–2408. <http://doi.org/10.1256/qj.03.178>.

1043 [Ptashnik2011] Ptashnik IV, Shine KP, Vigasin AA. Water vapour self-continuum and water dimers: 1.
1044 Analysis of recent work. J Quant Spectrosc Radiat Transfer 2011;112:1286–1303. [http://](http://doi.org/10.1016/j.jqsrt.2011.01.012)
1045 doi.org/10.1016/j.jqsrt.2011.01.012.

1046 [Ptashnik2012] Ptashnik IV, McPheat RA, Shine KP, Smith KM, Williams RG. Water vapour foreign-
1047 continuum absorption in near-infrared windows from laboratory measurements. Phil Trans R Soc A
1048 2012;370:2557–2577. <http://dx.doi.org/10.1098/rsta.2011.0218>.

1049 [Ptashnik2019] Ptashnik IV, Klimeshina TE, Solodov AA, Vigasin AA. Spectral composition of the water
1050 vapour self-continuum absorption within 2.7 and 6.25 μm bands. J Quant Spectrosc Radiat Transfer
1051 2019;228:97–105. <http://doi.org/10.1016/j.jqsrt.2019.02.024>.

1052 [Richard2017] Richard L, Vasilchenko S, Mondelain D, Ventrillard I, Romanini D, Campargue A. Water
1053 vapor self-continuum absorption measurements in the 4.0 and 2.1 μm transparency windows. J Quant
1054 Spectrosc Radiat Transfer 2017;201:171–179. <http://dx.doi.org/10.1016/j.jqsrt.2017.06.037>.

1055 [Scribano2007] Scribano Y, Leforestier C. Contribution of water dimer absorption to the millimeter and
1056 far infrared atmospheric water continuum. J. Chem. Phys. 2007;126:234301.
1057 <http://doi.org/10.1063/1.2746038>.

1058 [Serov2014] Serov EA, Koshelev MA, Odintsova TA, Parshin VV, Tretyakov MYu. Rotationally resolved
1059 water dimer spectra in atmospheric air and pure water vapour in the 188–258 GHz range. Phys Chem
1060 Chem Phys 2014;16:26221. <http://doi.org/10.1039/c4cp03252g>.

1061 [Serov2017] Serov EA, Odintsova TA, Tretyakov MYu, Semenov VE. On the origin of the water vapour
1062 continuum absorption within rotational and fundamental vibrational bands, J Quant Spectrosc Radiat
1063 Transfer 2017;193:1–12, <http://doi.org/10.1016/j.jqsrt.2017.02.011>.

1064 [Shine2012] Shine KP, Ptashnik IV, Rädcl G. The Water Vapour Continuum: Brief History and Recent
1065 Developments. Surv Geophys 2012;33:535-55. <http://dx.doi.org/10.1007/s10712-011-9170-y>.

1066 [Shine2016] Shine KP, Campargue A, Mondelain D, McPheat RA, Ptashnik IV, Weidmann D. The water
1067 vapour continuum in near-infrared windows – Current understanding and prospects for its inclusion in
1068 spectroscopic databases. J Mol Spectrosc 2016;327:193–208.
1069 <http://dx.doi.org/10.1016/j.jms.2016.04.011>.

1070 [Tipping1995] Tipping RH, Ma Q. Theory of water-vapour continuum and validations. Atmos Res
1071 1995;36:69-94. [http://dx.doi.org/10.1016/0169-8095\(94\)00028-C](http://dx.doi.org/10.1016/0169-8095(94)00028-C).

1072 [Tran2013] Tran H, Ngo NH, Hartmann J-M. Efficient computation of some speed-dependent isolated line
1073 profiles. J Quant Spectrosc Radiat Transfer 2013;129:199-203.
1074 <http://doi.org/10.1016/j.jqsrt.2013.06.015>.

1075 [Tran2014] Tran H, Ngo NH, Hartmann J-M. Erratum to “Efficient computation of some speed-dependent
1076 isolated line profiles”. J Quant Spectrosc Radiat Transfer 2014;134:104.
1077 <http://doi.org/10.1016/j.jqsrt.2013.10.015>.

1078 [Tran2017].Tran H, Li G, Ebert V, Hartmann J-M. Super- and sub-Lorentzian effects in the Ar-broadened
1079 line wings of HCl gas. J Chem Phys 2017;146:194305. <http://doi.org/10.1063/1.4983397>.

1080 [Tretyakov2013] Tretyakov MYu Serov EA, Koshelev MA, Parshin VV, Krupnov AF. Water Dimer
1081 Rotationally Resolved Millimeter-Wave Spectrum Observation at Room Temperature. Phys Rev Lett
1082 2013;110:093001. <http://doi.org/10.1103/PhysRevLett.110.093001>.

1083 [Tso1998] Tso HCW, Geldart DJW, Chýlek P. Anharmonicity and cross section for absorption of radiation
1084 by water dimer. J Chem Phys 1998;108:5319. <https://doi.org/10.1063/1.475967>

1085 [Vasilchenko2019] Vasilchenko S, Campargue A, Kassi S, Mondelain D. The water vapour self- and
1086 foreign-continua in the 1.6 μm and 2.3 μm windows by CRDS at room temperature, J Quant Spectrosc
1087 Radiat Transfer 2019;227:230–238. <http://doi.org/10.1016/j.jqsrt.2019.02.016>.

1088 [Wagner2020] Wagner G, Birk M, Tretyakov MYu. What we learn by subtracting Lorentzian line wings
1089 beyond 25 cm^{-1} from the MT_CKD H_2O continua. , J Quant Spectrosc Radiat Transfer, this issue.

1090

Declaration of interests

The authors declare that they have no known competing financial interests or personal relationships that could have appeared to influence the work reported in this paper.

The authors declare the following financial interests/personal relationships which may be considered as potential competing interests:

Author statement

Manfred Birk: Conceptualization, Methodology, Software, Formal analysis, Investigation, Writing - Original Draft, Writing - Review & Editing, Visualization, Supervision, Project administration, Funding acquisition

Georg Wagner: Conceptualization, Methodology, Software, Formal analysis, Investigation, Writing - Original Draft, Writing - Review & Editing, Visualization

J. Loos: Software, Investigation, Formal analysis, Writing - Original Draft

Keith P. Shine: Writing - Original Draft, Writing - Review & Editing